Symmetry, stability, and computation of degenerate lasing modes

David Liu,[1,2,*] Bo Zhen,[2] Li Ge,[3] Felipe Hernandez,[1] Adi Pick,[4]
Stephan Burkhardt,[5] Matthias Liertzer,[5] Stefan Rotter,[5] and Steven G. Johnson[1,2,†]

[1] *Department of Mathematics, Massachusetts Institute of Technology, Cambridge, Massachusetts 02139, USA*
[2] *Department of Physics, Massachusetts Institute of Technology, Cambridge, Massachusetts 02139, USA*
[3] *Department of Engineering Science and Physics, College of Staten Island, and The Graduate Center, CUNY, Staten Island, New York 10314, USA*
[4] *Department of Physics, Harvard University, Cambridge, Massachusetts 02138, USA*
[5] *Institute for Theoretical Physics, Vienna University of Technology (TU Wien), A-1040 Vienna, Austria*

arXiv:1611.01676v1 [physics.optics] 5 Nov 2016

We present a general method to obtain the stable lasing solutions for the steady-state *ab-initio* lasing theory (SALT) for the case of a degenerate symmetric laser in two dimensions (2d). We find that under most regimes (with one pathological exception), the stable solutions are clockwise and counterclockwise circulating modes, generalizing previously known results of ring lasers to all 2d rotational symmetry groups. Our method uses a combination of semi-analytical solutions close to lasing threshold and numerical solvers to track the lasing modes far above threshold. Near threshold, we find closed-form expressions for both circulating modes and other types of lasing solutions as well as for their linearized Maxwell–Bloch eigenvalues, providing a simple way to determine their stability without having to do a full nonlinear numerical calculation. Above threshold, we show that a key feature of the circulating mode is its "chiral" intensity pattern, which arises from spontaneous symmetry-breaking of mirror symmetry, and whose symmetry group requires that the degeneracy persists even when nonlinear effects become important. Finally, we introduce a numerical technique to solve the degenerate SALT equations far above threshold even when spatial discretization artificially breaks the degeneracy.

I. INTRODUCTION

Many lasers are formed from high-symmetry microcavity geometries that have degenerate resonant modes, most famously ring and disc resonators in which the clockwise and counterclockwise circulating modes are degenerate (having the same complex resonant frequency). In a linear system, any superposition of these solutions also satisfies Maxwell's equations, but above-threshold lasers have nonlinear gain that allows only certain superpositions; it is well known that the only stable lasing solutions of a ring are the circulating solutions $\mathbf{E} \sim e^{im\phi}$, as opposed to the standing-wave modes $\mathbf{E} \sim \sin m\phi$, $\cos m\phi$ [1–4]. However, more recent microcavities often have other symmetry groups supporting degeneracies [5], such as the 6-fold symmetry that commonly occurs in photonic-crystal resonators [6], as seen in Fig. (1), or more generally the $C_{n\mathrm{v}}$ symmetry group (n-fold rotations and n mirror planes) for $n > 2$ [5], and much less is known about the lasing solutions in such cases. Figure (1) gives examples of degenerate lasing modes in $C_{n\mathrm{v}}$ geometries. Previous work [7] showed how the steady-state degenerate solutions of SALT (steady-state ab-initio lasing theory [8–12]) could be found from an educated guess of a superposition of the threshold degenerate modes, and how their stability could be computed *numerically*. In this work, we show rigorously using degenerate perturbation theory on the SALT equations that the circulating modes used in Ref. [7], along with standing-wave modes that are linear combinations of the clockwise and counterclockwise circulating modes, are the *only* solutions to SALT in the $C_{n\mathrm{v}}$ degenerate case. We complement those results with semi-analytical *closed-form* expressions for the stability eigenvalues of the Maxwell–Bloch equations linearized about these lasing solutions (Sec. III). We find that the only stable solutions right above threshold (with one isolated exception that is unattainable under normal circumstances) are typically the circulating ones. An important observation of our paper is that $C_{n\mathrm{v}}$ symmetries experience a spontaneous symmetry breaking due to nonlinearity above threshold, and analysis of the resulting "chiral" symmetry [13] is key to stability of the lasing mode. These analytical solutions then give us a starting point for a *numerical* method to compute the degenerate solutions far above threshold, extending our earlier work on computational methods for non-degenerate SALT [14]. Our numerical method, in turn, relies on a new semi-analytical technique (Sec. V A) to address problems created by numerical symmetry breaking (e.g., by a low-symmetry computational grid) that would otherwise spoil the nonlinear SALT solutions.

In Ref. [7], a full linear-stability analysis (Sec. III B) was applied numerically to the Maxwell–Bloch equations of lasing in order to check whether the steady state was stable, and stability of the solution was also analyzed when the degeneracy was broken by a perturbation. This generalized many earlier works on ring-laser solutions and perturbations thereof [15–19]. It reproduced the stability of the circulating solution near threshold, and found that far above the lasing threshold (where nonlinearities are strong) the circulating solution may become unstable (replaced by an oscillating limit-cycle solution). Conversely,

* daveliu@mit.edu
† stevenj@math.mit.edu

it was found there that slightly breaking the symmetry caused the (now nearly degenerate) solution to become unstable (e.g., oscillating between clockwise and counterclockwise modes) in the vicinity of the threshold, but that a stable solution re-appears further above threshold by means of cooperative frequency locking [19, 20]. The present paper complements those results in two ways. First, near threshold, we are able to both *solve for* the steady-state lasing modes (Sec. III) and evaluate their stability (Sec. III B) *analytically*, by perturbation theory in the basis of the degenerate linear solutions at lasing threshold, and we generalize the notion of a circulating laser mode to other symmetry groups and establish its stability near threshold. Even the degeneracy itself is somewhat unusual above threshold, because the nonlinear gain spontaneously breaks some of the symmetry in noncircular ($C_{n\mathrm{v}}$ with $n \neq \infty$) geometries, leaving one with a "chiral" degeneracy as discussed in Sec. III B, Ref. [13], and Appendix B. Second, we develop a numerical solution technique for *far above* threshold in Sec. V A, generalizing earlier SALT methods, where a numerical nonlinear solver is the only option; in this regime, our focus is on finding a degenerate lasing mode in SALT (if one exists), and we defer to the results of Ref. [7] for checking its stability after a solution far above threshold is found.

Above threshold, the SALT equations [8, 10, 12] provide an elegant formulation of the problem of steady-state lasing modes: they analytically eliminate the time dependence from the Maxwell–Bloch equations to obtain a nonlinear Maxwell-like eigenproblem $\nabla \times \nabla \times \mathbf{E}_\mu = \omega_\mu^2 \varepsilon_{\mathrm{SALT}} \mathbf{E}_\mu$ for the lasing electric fields $\mathbf{E}_\mu$ and frequencies ω_μ, in which the permittivity $\varepsilon_{\mathrm{SALT}}$ depends nonlinearly on both the field and frequency (here, the speed of light c has been set to unity). This equation can be efficiently solved numerically by adapting standard techniques from computational electromagnetism [14]. As described below and also in previous work [2, 7], the SALT framework applies very naturally to lasing of degenerate microcavities, assuming a stable degenerate steady state exists, but it turns out that there are two complications. First, in order to apply a numerical nonlinear solver to a large system of nonlinear equations like SALT, one needs to have a good "starting guess" for the solution. In the non-degenerate case, the starting guess is supplied by the threshold solution, but for a degenerate threshold there are infinitely many superpositions. Picking the wrong starting guess, e.g., the $\sin(m\phi)$ mode in a ring, would lead SALT to converge to an unstable solutions, but our near-threshold perturbutation theory supplies us with a correct guess (which turns out to be the $C_{n\mathrm{v}}$ analog of the circulating solution in the ring).

Second, there is a tricky complication that arises purely from *numerical* effects when a practical computational method is applied to spatially discretize the SALT equations. In principle, what one would like to find from a degenerate SALT solver is a lasing mode (e.g., the clockwise circulating mode of a ring) with a passive pole (a pole of the Green's function linearized around the lasing solution) that coincides with the lasing frequency (there will be two possible lasing modes, e.g., clockwise and counterclockwise, but only one solution can exist at a time with nonzero amplitude due to the nonlinearity; which one is found will depend on the starting "guess" of the SALT solver). However, when one discretizes a microcavity geometry for a numerical solver, e.g., in a finite-difference or finite-element method, often the discretization itself breaks the symmetry and hence breaks the degeneracy slightly, causing the passive pole to separate from the lasing frequency. In a linear eigenproblem, this is at worst a minor annoyance, because from the symmetry group

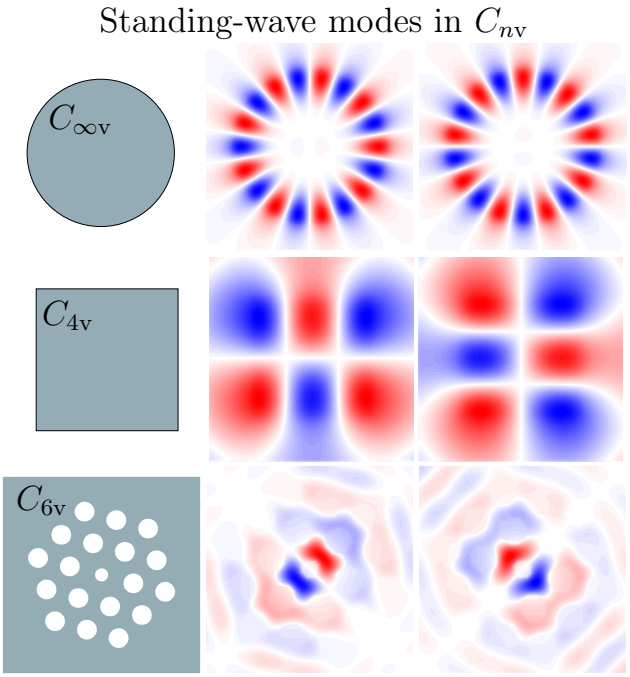

Figure 1. (Color online) Degenerate pairs of standing-wave modes in a laser. For this uniform dielectric disk (top), which has $C_{\infty\mathrm{v}}$ symmetry, the two eigenfunctions (of which only the real part is shown) are proportional to $\cos(\ell\phi)$ and $\sin(\ell\phi)$ (here, $\ell = 9$). For a homogeneous dielectric square ($\varepsilon = 5$ inside a square of length 1), the eigenfunctions are $\frac{\pi}{2}$ rotations of one another. Here, the order of the irreducible representation (irrep) is $\ell = 1$, which is the only possibility for $C_{4\mathrm{v}}$. The $\frac{\pi}{2}$ rotation is an exact symmetry of the geometry, so there is an exact degeneracy even for the numerical grid. For $C_{6\mathrm{v}}$, the symmetry group of the regular hexagon, as in this example of TE modes (with the transverse magnetic field H_z shown) in a 2d slab with air holes (described in further detail in Sec. V B), the two eigenfunctions have no immediately obvious symmetry operation that transforms between them, but are in fact still degenerate (here $\ell = 1$, and there also exists an $\ell = 2$ irrep with its own degenerate pair). In all three cases (and in fact for all $C_{n\mathrm{v}}$), the standing-wave modes have mirror planes that are $\frac{\pi}{2}$ rotations from one another, and the two standing-wave modes have opposite parities across these mirror planes.

one can easily identify resonance modes that "should" be degenerate [5, 21]. In the nonlinear problem, however, the splitting can prevent the desired solution (e.g., the circulating mode) from existing in the SALT equations, because the solver can no longer pick arbitrary superpositions of the formerly degenerate modes, as described in Sec. V A. (If the discretization breaks the degeneracy, but the pump strength is high enough, a single-mode circulating solution *may* still come back into existance, due to strong nonlinear self-interaction effects [7]. This effect can provide a fast and easy way to initially evaluate the field profile of a discretized geometry that is not exactly symmetric, and hence does not have an exact degeneracy. However, the conditions under which this effect can happen are not completely understood, as we explain in Sec. V, and we wish to deal with the discretization symmetry breaking in a more systematic and provably reliable manner.) To fix the problem of broken degeneracy from discretization, we found a simple way to uniquely restore the degeneracy in a way that both guarantees convergence to the correct solution (as the discretization is refined), that generalizes to an arbitrary number of lasing modes (in Sec. V C), and that is, at worst, a few times more computationally expensive than our non-degenerate solver.

II. BACKGROUND

A. Review of SALT

The equations of SALT are derived from the Maxwell–Bloch equations [22–25] (with the rotating-wave approximation):

$$\begin{aligned} -\varepsilon\ddot{\mathbf{E}}^{+} &= \nabla\times\nabla\times\mathbf{E}^{+}+\ddot{\mathbf{P}}^{+} \\ i\dot{\mathbf{P}}^{+} &= (\omega_a - i\gamma_\perp)\mathbf{P}^{+}+\gamma_\perp\mathbf{E}^{+}D \\ \dot{D} &= \gamma_\parallel(D_0-D)+\mathrm{Im}(\mathbf{E}^{-}\cdot\mathbf{P}^{+}), \end{aligned} \tag{1}$$

where $\mathbf{E}^{+}(\mathbf{x},t)$ is the "positive-frequency" component of the electric field [with $\mathbf{E}^{-}=\mathbf{E}^{+\star}$ and the physical field given by $2\mathrm{Re}(\mathbf{E}^{+})$], $\varepsilon(\mathbf{x})$ is the "cold-cavity" permittivity (not including the gain transition), $\mathbf{P}(\mathbf{x},t)$ is the polarization describing a transition (of frequency ω_a and linewidth $\gamma_\perp$) between two atomic energy levels, $D(\mathbf{x},t)$ is the population inversion between those two levels (with relaxation rate $\Gamma_\parallel$), and $D_0(\mathbf{x})$ is the strength of a pumping process driving the inversion. Additionally, for convenience, one chooses units such that the following factors are set to unity: the dipole moment matrix element of the two level system, Planck's constant $\hbar$, and the speed of light c. Using the stationary inversion approximation $D(\mathbf{x},t)\approx D(\mathbf{x})$ [8, 26] along with an ansatz of a finite number of lasing modes

$$\mathbf{E}^{+}(\mathbf{x},t)=\sum_\nu \mathbf{E}_\nu(\mathbf{x})e^{-i\omega_\nu t}, \tag{2}$$

where ω_ν are the real mode frequencies, the second equation in Eq. (1) is solved to eliminate $\mathbf{P}^{+}$ as an unknown, and the third equation becomes

$$\dot{D}=\gamma_\parallel(D_0-D)+D\,\mathrm{Im}\left[\sum_{\mu\nu}\Gamma(\omega_\nu)\mathbf{E}_\mu^{\star}\cdot\mathbf{E}_\nu e^{i(\omega_\mu-\omega_\nu)t}\right], \tag{3}$$

where $\Gamma(\omega_\mu)\equiv\gamma_\perp/(\omega_\mu-\omega_a+i\gamma_\perp)$. In order for the stationary inversion approximation $\dot{D}=0$ to be valid, the oscillating terms on the right-hand side of Eq. (3) must average to zero on a timescale much faster than the relaxation timescale $1/\gamma_\parallel$; and in order to do so, the beating frequencies $\omega_\mu-\omega_\nu$ must be either exactly zero or much faster than the relaxation rate $\gamma_\parallel$ [8, 12, 26]. This condition is evidently true when any pair of modes is either exactly degenerate, or situated very far apart from each other in frequency space. When these conditions are met, Eq. (1) reduces to the SALT equation [8, 10, 12]

$$\nabla\times\nabla\times\mathbf{E}_\mu=\omega_\mu^2\left[\varepsilon+\Gamma(\omega_\mu)D\right]\mathbf{E}_\mu, \tag{4}$$

for the unknowns $\mathbf{E}_\mu$ and ω_ν, where $D(\mathbf{x})$ is the steady-state population inversion, which depends nonlinearly on the electric fields and lasing frequencies of all lasing modes:

$$D(\mathbf{x})=\frac{D_0(\mathbf{x})}{1+\gamma_\parallel^{-1}\sum_\nu|\Gamma(\omega_\nu)\mathbf{E}_\nu|^2}. \tag{5}$$

The intensity term in the denominator of Eq. (5) is known as the "spatial hole-burning" [8, 24, 26] term; it represents the saturation of the gain medium due to the total time-averaged intensity of all the lasing modes. Once Eq. (4) is solved for all the lasing modes $\mathbf{E}_\mu$ and frequencies ω_μ, one typically checks that the "passive" poles, i.e. the eigenvalues $\tilde{\omega}_\mu$ of the linearized SALT equation

$$\nabla\times\nabla\times\tilde{\mathbf{E}}_\mu=\tilde{\omega}_\mu\left[\varepsilon+\Gamma(\tilde{\omega}_\mu)D\right]\tilde{\mathbf{E}}_\mu, \tag{6}$$

are not above the real axis. As long as $|\omega_\nu-\tilde{\omega}_\mu|\gg\gamma_\parallel$ (where ω_ν are the lasing frequencies), this is a good indicator that the SALT solution is stable. However, a rigorous evaluation of the stability of the SALT solution requires a linear stability analysis based on the MB equations [7]. (In Sec. III B, we give analytical results for this stability analysis for the near-threshold degenerate case.)

B. Effects of exact degeneracies

So far, most cases in which SALT has been applied have dealt with either single lasing modes or multimode regimes in which frequencies are far apart. When two lasing frequencies are close but not exactly degenerate, there is non-negligible beating and SALT is invalid. However, when two lasing modes are *exactly* degenerate, we find

that SALT is still perfectly valid, because there is an exact steady-state solution of the MB equations (for a single lasing mode), provided that interference between the two degenerate modes is taken into account. Of course, it is possible that a degeneracy in the linear regime may split in the presence of the laser nonlinearity above threshold. However, if a degeneracy persists (and we have observed that it is guaranteed to do so for $C_{n\mathrm{v}}$ symmetry-induced degeneracies, because of the "chiral" symmetry of the lasing mode as discussed in Appendix. A), our method will find it. The literature on degenerate lasing modes has almost invariably dealt with whispering-gallery modes in microdisks and ring resonators [1–4]. Many of these earlier works discussed the stability of traveling-wave modes in ring resonators under perturbations that break the symmetry [15–19]. A very limited number of other works on degenerate lasing modes in other geometries exist [27], which were mostly experimental and focused on the linear cavity rather than the nonlinear lasing regime. However, the microdisk is just one of many examples of a setting where one can find degenerate resonant modes that can lase: there are a great variety of other symmetric geometries where degeneracies can occur [5, 21, 28]. So far, the problem of above-threshold degenerate modes in lasers has not been studied systematically for the general $C_{n\mathrm{v}}$ case.

The presence of degenerate eigenvalues is typically a direct consequence of symmetry. For systems with $C_{n\mathrm{v}}$ symmetry for $n > 2$ (n-fold rotational symmetry with n mirror planes, the symmetry of the regular n-gon), the existence of 2d irreducible representations (irreps) of the symmetry group corresponds to 2-fold degeneracies. Below, we therefore refer to 2-fold degenerate modes (at lasing threshold) as corresponding to a 2d irrep, and we exploit some known properties of these irreps in deriving selection rules [5] for overlap integrals. For systems with C_n symmetry (n-fold rotational symmetry without mirror symmetry, e.g., a "chiral" spiral structure with n arms), the combination of group theory and electromagnetic reciprocity again supports 2-fold degenerate solutions [13] (see also Appendix A for a review). Even with $C_{n\mathrm{v}}$ symmetry, we explain below that the nonlinear hole-burning term for lasers above threshold typically breaks the mirror symmetry, so the reciprocity argument for C_n symmetry is crucial to maintaining the degeneracy of the lasing mode and a passive pole. Figure (1) shows three examples of symmetric geometries, along with examples of degenerate eigenfunctions.

Ordinarily, SALT assumes that all distinct modes have distinct frequencies, i.e. $\omega_\mu \neq \omega_\nu$ when $\mu \neq \nu$, which gives the stationary-inversion expression Eq. (5) when higher-frequency $\omega_\mu - \omega_\nu$ ($\nu \neq \mu$) terms are dropped. However, when there are degeneracies, the MB equations will have terms of the form $\mathbf{E}_\mu \cdot \mathbf{E}_\nu^\star$ where $\mu \neq \nu$, since $\omega_\mu = \omega_\nu$ and one can no longer drop the $e^{i(\omega_\mu - \omega_\nu)t}$ term. The correct expression for the stationary inversion will then be

$$D = \frac{D_0}{1 + \gamma_\parallel^{-1} \sum{}' \Gamma_\mu \mathbf{E}_\mu \cdot \Gamma_\nu^\star \mathbf{E}_\nu^\star}, \tag{7}$$

where $\Gamma_\mu \equiv \Gamma(\omega_\mu)$ and $\sum{}'$ indicates a summation over all μ and ν for which $\omega_\mu = \omega_\nu$, not just for $\mu = \nu$. To illustrate the difference between the two, we examine a case in which there are three lasing modes, two of which are degenerate with each other ($\omega_1 = \omega_2 \neq \omega_3$). Equation (5) will have

$$|\Gamma_1 \mathbf{E}_1|^2 + |\Gamma_2 \mathbf{E}_2|^2 + |\Gamma_3 \mathbf{E}_3|^2 \tag{8}$$

in the denominator, while Eq. (7) will have

$$|\Gamma_1 (\mathbf{E}_1 + \mathbf{E}_2)|^2 + |\Gamma_3 \mathbf{E}_3|^2 . \tag{9}$$

From Eq. (9) we see that the degenerate pair acts as a single mode that is a superposition of $\mathbf{E}_1$ and $\mathbf{E}_2$. This means that the solution to the lasing degenerate problem can be portrayed in two equivalent pictures. First, we can think of the linear combination $\mathbf{E} = \mathbf{E}_1 + \mathbf{E}_2$ as a single mode that satisfies the equation

$$\begin{aligned} -\nabla \times \nabla \times \mathbf{E} &= \omega_1^2 \left(\varepsilon + D\Gamma_1\right) \mathbf{E} \\ D &\equiv \frac{D_0}{1 + \gamma_\parallel^{-1} \left(|\Gamma_1 \mathbf{E}|^2 + |\Gamma_3 \mathbf{E}_3|^2 \right)} \end{aligned} \tag{10}$$

[where the external pump $D_0(\mathbf{x})$ may be spatially dependent, as noted before]. Second, we can think of the two modes as *separately* satisfying the two equations

$$\begin{aligned} -\nabla \times \nabla \times \mathbf{E}_{1,2} &= \omega_1^2 \left(\varepsilon + D\Gamma_1\right) \mathbf{E}_{1,2} \\ D &\equiv \frac{D_0}{1 + \gamma_\parallel^{-1} \left(|\Gamma_1 (\mathbf{E}_1 + \mathbf{E}_2)|^2 + |\Gamma_3 \mathbf{E}_3|^2 \right)}. \end{aligned} \tag{11}$$

The existence of a solution to Eq. (10) is a necessary but not sufficient condition for the existence of a solution to Eq. (11). The reason is that Eq. (11) enforces a double eigenvalue of the linearized eigenproblem (i.e. a double pole of the Green's function) on the real-ω axis, whereas Eq. (10) only enforces a single eigenvalue.

Prior to lasing, suppose that we have a 2-fold degenerate solution, corresponding to a double pole in the Green function. As the gain increases, and even when the system passes threshold and becomes nonlinear, poles can shift (and degeneracies may split) but poles do not appear or disappear discontinuously, so we should always expect there to be two poles (in the linearized Green's function around the SALT solution) arising from the original degenerate pair. Given this fact, if we solve the single-mode SALT equations as in Eq. (10), there is the danger that the other pole is unstable. As we show in Appendix. C, close to lasing threshold the zeroth order stability analysis (in the pump strength increment) simply depends on the SALT eigenproblem: if a SALT pole

lies above the real-ω axis, then a lasing solution is necessarily unstable, whereas SALT poles below the real axis cannot induce instability. If a pole lies *on* the real axis, higher-order calculations are required to check stability as described in Sec. III B.

On the other hand, if we find a solution of the two-mode SALT equations as in Eq. (11), then by construction we have placed both poles together on the real-ω axis and the other passive pole by itself is not a source of instability (and the overall stability of the Maxwell–Bloch equations can be checked as in Ref. [7]). However, Eq. (11) has a drawback: the hole-burning term now depends on the relative phase of $\mathbf{E}_1$ and $\mathbf{E}_2$. In the original SALT equations, even for multimode problems, the phase was irrelevant and was chosen arbitrarily in order to obtain a solvable system of equations. If we remove the arbitrary phase choice, our equations (derived in Ref. [14]) become underdetermined. However, if we solve the single-mode equation (Eq. (10)) but simultaneously constrain the other pole (the linearly independent degenerate partner) to be degenerate with the lasing pole, then we will effectively have solved Eq. (11), and in the following sections we will explain how to implement this constraint.

III. THRESHOLD PERTURBATION THEORY

In this section, we analyze the SALT (Eq. (4)) and Maxwell–Bloch equations (Eq. (1)) just above the lasing threshold in order to obtain insight into the nature of the degenerate solutions, as well as to determine the correct initial guess for the above-threshold regime (e.g., when solving for lasing modes using the method of Ref. [14]). For a regime with a single steady-state lasing mode $\mathbf{E}^+(\mathbf{x},t) = \mathbf{E}(\mathbf{x})e^{-i\omega t}$ with frequency ω, one obtains a stationary inversion [8, 10, 12] $D(\mathbf{x},t) = D(\mathbf{x})$ and the single-mode SALT nonlinear eigenproblem

$$\nabla\times\nabla\times\mathbf{E} = \omega^2\left[\varepsilon + \frac{D_0\Gamma(\omega)}{1+\gamma_\parallel^{-1}\left|\Gamma(\omega)\mathbf{E}\right|^2}\right]\mathbf{E}. \qquad (12)$$

The first lasing threshold occurs when D_0 is increased to a value D_t where a complex eigenvalue ω of this SALT equation with infinitesimal $\mathbf{E}$ hits the real-ω axis ($\mathrm{Im}\,\omega = 0$) [8, 12].

Now, we will consider the *near-threshold* problem $D_0 = D_\mathrm{t}(1+d)$ for $0 \le d \ll 1$, for the case where the threshold mode ($d = 0$) is doubly degenerate, and expand the solutions to lowest order in d. First (Sec. III A), we will solve the SALT equations perturbatively in d, in order to find the steady-state lasing solutions near threshold, regardless of whether they are stable. Then (Sec. III B), we will plug those solutions into the full Maxwell–Bloch equations, again expanding to lowest-order in d, in order to evaluate the dynamical stability of the SALT modes. This yields a small 4×4 eigenproblem, whose eigenvalues determine the stability, and whose matrix elements are integrals of the threshold solutions. In the case of $C_{n\mathrm{v}}$ symmetry, we know enough about the modes in order to simplify many of these calculations analytically, to conclude: (i) the only SALT solutions are either standing-wave or circulating solutions (defined below); (ii) the standing-wave modes are unstable for all $C_{n\mathrm{v}}$ cases (except for a small group of isolated, realistically unattainable examples when n is a multiple of four), and otherwise the stability can be determined by evaluating a simple integral of the threshold modes.

A. Perturbative lasing solutions near threshold

We begin with the situation of a degenerate threshold, where two modes $\mathbf{E}_1$ and $\mathbf{E}_2$ (such as any of the pairs in Fig. (1)) hit threshold at the same pump strength D_t and same frequency ω_t. Since the frequencies are the same, we can consider any linear superposition of the two modes as a single mode. With infinitesimal amplitude, Eq. (12) is

$$\nabla\times\nabla\times\mathbf{E}_{1,2} = \omega_\mathrm{t}^2\left(\varepsilon + D_\mathrm{t}\Gamma_\mathrm{t}\right)\mathbf{E}_{1,2}, \qquad (13)$$

where $\Gamma_\mathrm{t} = \Gamma(\omega_\mathrm{t})$. Now we perturb the pump strength to bring the mode slightly above threshold, with $D_0 = D_\mathrm{t}(1+d)$ and $0 < d \ll 1$. We then expect the lasing mode slightly above threshold to be of the form

$$\begin{aligned}\mathbf{E} &= \Gamma_\mathrm{t}^{-1}\sqrt{\gamma_\parallel d}\,(a_1\mathbf{E}_1 + a_2\mathbf{E}_2) + d^{3/2}\delta\mathbf{E},\\ \omega &= \omega_\mathrm{t} + \omega_1 d + \mathcal{O}(d^2)\end{aligned} \qquad (14)$$

where the complex coefficients $a_{1,2}$ and the real eigenvalue shift ω_1 are to be determined. The linear relation between d and intensity $|\mathbf{E}|^2$ has previously been shown for lasing modes above threshold in SPA-SALT approximation [12]. Inserting Eq. (14) into Eq. (12), expanding to lowest order in d, and taking the inner product of both sides with $\mathbf{E}_1$ and $\mathbf{E}_2$ (as performed in detail in Appendix B), we obtain the pair of nonlinear equations for $a_{1,2}$ and ω_1:

$$\begin{aligned}0 = \int d^3x\,\mathbf{E}_{1,2}\cdot(a_1\mathbf{E}_1 + a_2\mathbf{E}_2)\times\\ \left[\omega_1\frac{\partial}{\partial\omega_\mathrm{t}}\omega_\mathrm{t}^2(\varepsilon + D_\mathrm{t}\Gamma_\mathrm{t}) + \omega_\mathrm{t}^2 D_\mathrm{t}\Gamma_\mathrm{t}\left(1 - \left|a_1\mathbf{E}_1 + a_2\mathbf{E}_2\right|^2\right)\right]\end{aligned} \qquad (15)$$

To proceed, we must choose a basis $\mathbf{E}_{1,2}$ to work with (the end result, Eq. (14) turns out to be independent of the choice, as expected). One possible choice is the even and odd (with respect to the mirror planes of the $C_{n\mathrm{v}}$ geometry) standing-wave modes, which we denote as $\mathbf{E}_\mathrm{even}$ and $\mathbf{E}_\mathrm{odd}$ (as in Fig. (1)). However, it turns out that another choice makes the analytical solution of Eq. (15) significantly easier to obtain, due to various convenient symmetry properties. In particular, we construct a basis of *clockwise* and *counterclockwise* "circulating" modes

(analogous to $e^{\pm i\ell\phi}$ modes in a ring)

$$\mathbf{E}_\pm = \sum_{k=1}^{n} \exp\left(\pm\frac{2\pi i\ell k}{n}\right) R_{k/n}\mathbf{E}_{\rm even}, \qquad (16)$$

where ℓ is given by the 2d irrep that $\mathbf{E}_{\rm even}$ belongs to [ℓ ranges from 1 to floor($\frac{n-1}{2}$)], and $R_{k/n}$ is a counterclockwise rotation of the vector field $\mathbf{E}_{\rm even}(\mathbf{x})$ in the plane of the $C_{n\rm v}$ symmetry by $2\pi k/n$ (if ℓ is chosen to be the wrong integer, then $\mathbf{E}_\pm$ vanishes because Eq. (16) is a projection operator [5, 21]). With this definition, $\mathbf{E}_+$ and $\mathbf{E}_-$ are mirror flips of one another, and they span the same space as $\mathbf{E}_{\rm even}$ and $\mathbf{E}_{\rm odd}$. One important property of the $\mathbf{E}_\pm$ is that they transform according to the chiral $1d$ irreps of the C_n symmetry group, i.e. $R_{1/n}\mathbf{E}_\pm = \exp\left(\mp\frac{2\pi i\ell k}{n}\right)\mathbf{E}_\pm$. This fact will turn out to greatly simplify some upcoming calculations. Choosing $\mathbf{E}_1 = \mathbf{E}_+$ and $\mathbf{E}_2 = \mathbf{E}_-$ and exploiting the symmetry properties of this basis, we see (as shown in detail in Appendix B) that Eq. (15) reduces to

$$0 = a_\mp\left(\omega_1 H + G_D\right) - a_\mp\left|a_\pm\right|^2(I+J) - a_\mp\left|a_\mp\right|^2 I - a_\pm^2 a_\mp^\star K, \quad (17)$$

where the coefficients G_D, H, I, J, and K are simple overlap integrals of the threshold modes, given in closed form in Eq. (B5) and Eq. (B6). Equation. (17) can be solved in closed form (as performed in Appendix B), and yields only a few solutions. First, there are the purely circulating modes, given by

$$\mathbf{E} = \Gamma_{\rm t}^{-1}\sqrt{\frac{\left(\omega_1 H + G_D\right)\gamma_\parallel d}{I}}\mathbf{E}_\pm$$
$$\omega_1 = -\frac{{\rm Im}\left(G_D/I\right)}{{\rm Im}\left(H/I\right)}. \qquad (18)$$

The other solutions to Eq. (17) are *standing-wave* modes, as to be expected, and it turns out their form depends (as explained in Appendix B) crucially on whether the irrep of the degenerate pair satisfies $n = 4\ell$, where again ℓ is the order of the 2d irrep. For $C_{n\rm v}$ with $n \neq 4\ell$, the other modes are

$$\mathbf{E} = \Gamma_{\rm t}^{-1}\sqrt{\frac{(\omega_1 H + G_D)\gamma_\parallel d}{2I+J}}\left(\mathbf{E}_+ + e^{i\theta}\mathbf{E}_-\right)$$
$$\omega_1 = -\frac{{\rm Im}\left(G_D/[2I+J]\right)}{{\rm Im}\left(H/[2I+J]\right)} \qquad (19)$$

where θ is an arbitrary phase angle. (During numerical solution of Eq. (12), we have found that for some n, there seem to be constraints on θ, namely having to be a multiple of $\frac{\pi}{n}$. These constraints probably come from equations that are higher-order in d than our perturbation theory. However, they are inconsequential because it turns out that these standing-wave modes are always unstable, regardless of θ.) On the other hand, for the case of $n = 4\ell$, there are *two* sets of standing-wave modes. The first is

$$\mathbf{E} = \Gamma_{\rm t}^{-1}\sqrt{\frac{(\omega_1 H + G_D)\gamma_\parallel d}{2I+J+K}}\left(\mathbf{E}_+ \pm \mathbf{E}_-\right)$$
$$\omega_1 = -\frac{{\rm Im}\left(G_D/[2I+J+K]\right)}{{\rm Im}\left(H/[2I+J+K]\right)} \qquad (20)$$

and the other is

$$\mathbf{E} = \Gamma_{\rm t}^{-1}\sqrt{\frac{(\omega_1 H + G_D)\gamma_\parallel d}{2I+J-K}}\left(\mathbf{E}_+ \pm i\mathbf{E}_-\right)$$
$$\omega_1 = -\frac{{\rm Im}\left(G_D/[2I+J-K]\right)}{{\rm Im}\left(H/[2I+J-K]\right)}. \qquad (21)$$

These four sets of solutions turn out to constitute all the solutions of Eq. (17) for the general $C_{n\rm v}$ case, and this completes the solution of Eq. (12) slightly above threshold. Figure. (2) shows a comparison of numerical results for a 1d $C_{5\rm v}$ laser with the predictions of perturbation theory.

In order to find out which of these solutions is the one that actually lases in a real $C_{n\rm v}$ system, we must test stability of each of these solutions. It turns out that this test can also be done mostly analytically, using perturbation theory on the linearized Maxwell–Bloch equations, as we will present in the next section.

B. Perturbative stability analysis

While these three forms of lasing modes all solve SALT near threshold, and hence are "fixed-point" equilibria of the Maxwell–Bloch equations, one intuitively expects that only the circulating mode will be stable. The reason is that standing-wave modes for the $C_{n\rm v}$ group have zero amplitude along certain lines, most obviously along $x = 0$ for the $\mathbf{E}_{\rm odd}$ mode, and those zero-amplitude regions are making no use of the gain. This allows the opposite-symmetry standing-wave mode to grow exponentially into these nulls, and this is the reason why the sine and cosine modes are unstable in a ring. (This fact is only true for *exact* degeneracies; for real systems, which almost always break the degeneracy, there may be small regions near threshold where the standing-wave mode is stable [29].) To quantify this intuition, we perform linear-stability analysis, along the same lines as the numerical procedure in Ref. [7]. We linearize the Maxwell–Bloch equations for small perturbations around the SALT modes, by inserting

$$\mathbf{E}^+(\mathbf{x},t) = \left[\mathbf{E}(\mathbf{x}) + \delta\mathbf{E}(\mathbf{x},t)\right]e^{-i\omega t}$$
$$\mathbf{P}^+(\mathbf{x},t) = \left[\mathbf{P}(\mathbf{x}) + \delta\mathbf{P}(\mathbf{x},t)\right]e^{-i\omega t} \qquad (22)$$
$$D(\mathbf{x},t) = D(\mathbf{x}) + \delta D(\mathbf{x},t)$$

into the Maxwell–Bloch equations (where $\mathbf{E}$ is any of the SALT solutions obtained in Sec. III A, $D(\mathbf{x})$ is the stationary inversion given in (12), ω is the lasing frequency

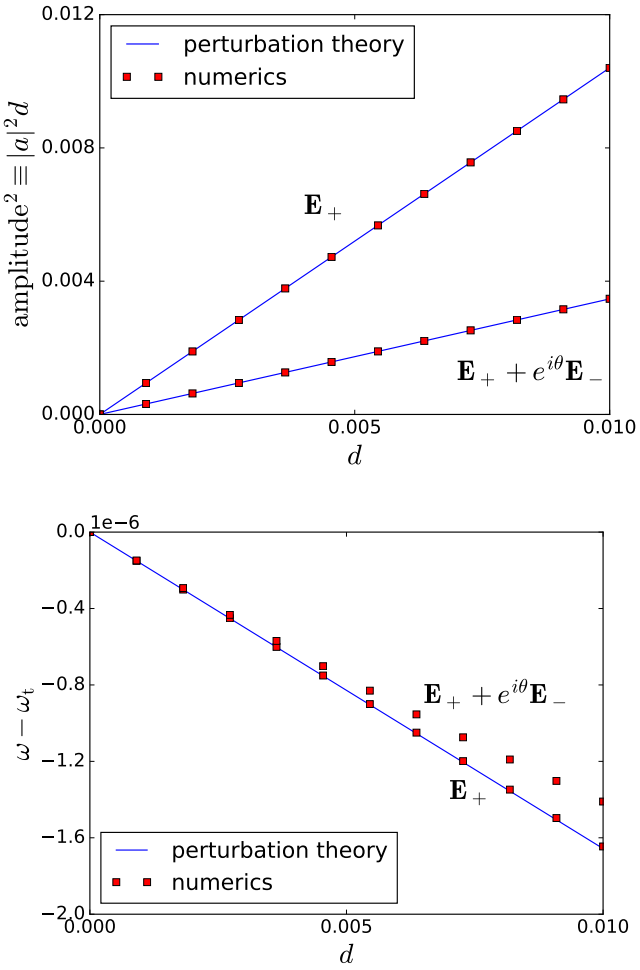

Figure 2. (Color online) Lasing amplitudes (top) and frequency shifts (bottom) for 1d laser (periodic geometry with $0 < x < 1$) with uniform dielectric $\varepsilon(x) = 1 + 0.3i$ and gain profile $D_0(x) = D_t(1+d)[1 + 0.2\cos(2\pi n x)]$. Here, we have chosen $n = 5$, so the gain has C_{5v} symmetry, and the discretization had $N = 150$ grid points. Data points were obtained by solving Eq. (12) (SALT) numerically using Newton's method [14], while theoretical lines were provided by Eq. (18) and Eq. (19). For the standing mode, numerical results are independent of relative phase θ, as predicted by Eq. (19). Agreement between numerics and theory is excellent for mode amplitudes (up to at least $d \approx 100$ [not shown in the figure], and possibly much higher) but only good at $d < 0.005$ for frequency shifts. For the numerical data in the amplitude plot, only the magnitude of the $\mathbf{E}_+$ component (obtained by taking the normalized inner product of the lasing mode $\mathbf{E}$ with $\mathbf{E}_+$) of both the circulating and standing-wave modes are shown. For the $\mathbf{E}_-$ component, the circulating mode had magnitude zero and the standing mode had the same magnitude as the $\mathbf{E}_+$ component.

given in Eq. (14), and $\mathbf{P}(\mathbf{x}) = \Gamma(\omega)\mathbf{E}(x)D$, is the polarization field. We collect terms order-by-order in the perturbations δ. The zeroth-order equations are simply the SALT equations and are already satisfied by construction by $\mathbf{E}$, $\mathbf{P}$, and $D(\mathbf{x})$. The first-order equations are

$$\begin{aligned} 0 &= -\nabla\times\nabla\times\delta\mathbf{E} + \left(\frac{d}{dt} - i\omega\right)^2(\varepsilon\delta\mathbf{E} + \delta\mathbf{P}) \\ i\delta\dot{\mathbf{P}} &= (\omega_a - \omega - i\gamma_\perp)\delta\mathbf{P} + \gamma_\perp(D\delta\mathbf{E} + \mathbf{E}\delta D) \\ \delta\dot{D} &= -\gamma_\parallel\delta D + \mathrm{Im}(\mathbf{P}\cdot\delta\mathbf{E}^\star + \mathbf{E}^\star\cdot\delta\mathbf{P}). \end{aligned} \tag{23}$$

Eq. (23) can be written as a matrix equation

$$\left(\mathsf{C}\frac{d^2}{dt^2} + \mathsf{B}\frac{d}{dt} + \mathsf{A}\right)\mathsf{u}(t) = 0 \tag{24}$$

or alternatively as quadratic eigenvalue problem [30]

$$\left(\mathsf{C}\sigma^2 + \mathsf{B}\sigma + \mathsf{A}\right)\mathsf{x} = 0 \tag{25}$$

where the unknown vector is

$$\mathsf{u}(t) = \begin{pmatrix} \mathrm{Re}\,\delta\mathbf{E} \\ \mathrm{Im}\,\delta\mathbf{E} \\ \mathrm{Re}\,\delta\mathbf{P} \\ \mathrm{Im}\,\delta\mathbf{P} \\ \delta\mathbf{D} \end{pmatrix} = \mathrm{Re}\left(\mathsf{x}e^{\sigma t}\right). \tag{26}$$

The goal of the stability analysis is to find the eigenvalues σ for a given lasing mode $\mathbf{E}$. If the real part of any of the eigenvalues σ is positive, then the lasing mode is unstable, while if all the eigenvalues have non-positive real parts, then the lasing mode is stable (with some technical care required for zero eigenvalues and structural stability, described in Appendix C). Ref. [7] discretized Eq. (23) to obtain Eq. (25) and then solved the resulting matrix equation numerically to find the eigenvalues σ and hence evaluated the SALT stability for any pump strength above threshold. Here, we focus on the regime slightly above threshold, and show that the equations can be solved analytically to lowest order in d, and this is enough to evaluate near-threshold stability. We begin by noting that the matrices can be expanded as

$$\begin{aligned} \mathsf{A} &= \mathsf{A}_0 + \mathsf{A}_{1/2}\sqrt{d} + \mathsf{A}_1 d + \mathcal{O}(d^{3/2}) \\ \mathsf{B} &= \mathsf{B}_0 + \mathsf{B}_1 d + \mathcal{O}(d^2) \\ \mathsf{C} &= \mathsf{C}_0 \end{aligned} \tag{27}$$

(where d is the relative pump increment above threshold, as introduced in Sec. III), since the matrices come from the coefficients of Eq. (23) and contain the lasing solutions $\mathbf{E}$ and other associated fields $\mathbf{P}$ and D. As a result, the eigenvalues and eigenvectors can also be expanded this way:

$$\begin{aligned} \mathsf{x} &= \mathsf{x}_0 + \mathsf{x}_{1/2}\sqrt{d} + \mathsf{x}_1 d + \mathcal{O}(d^{3/2}) \\ \sigma &= \sigma_0 + \sigma_{1/2}\sqrt{d} + \sigma_1 d + \mathcal{O}(d^{3/2}). \end{aligned} \tag{28}$$

We insert Eqs. (27) and (28) into Eq. (25) and solve order-by-order in $\sqrt{d}$ until a non-zero σ is found, as explained in detail in Appendix C. At zeroth order, Eq. (25) is equivalent to the SALT equation at threshold

(Eq. (13)), and has two kinds of solutions. First, there are the below threshold "passive" modes [8, 12], which have $\mathrm{Re}(\sigma_0) < 0$ (because for these modes, σ_0 is simply the difference $\tilde{\omega} - \omega_\mathrm{t}$ between the complex pole $\tilde{\omega}$ of the passive mode and the real threshold frequency ω_t) and hence are stable. Therefore, when d is small enough, we can say for certain that having one of these σ_0 above the real axis would make the system unstable, so having all passive poles of the SALT equation be below the real axis is a *necessary* condition for lasing near threshold, for small d. (Far above threshold, however, this is no longer true, as shown in Ref. [7].) Second, from the degenerate *threshold* modes, we obtain

$$\begin{aligned} \sigma_0 &= 0 \\ \mathsf{x}_0 &= \sum_{k=1}^{4} b_k \mathsf{v}_k, \end{aligned} \tag{29}$$

where b_k are arbitrary complex coefficients that will be determined later at higher order (similarly to linear degenerate perturbation theory in quantum mechanics [31]), and the vectors v_k are

$$\mathsf{v}_k = \begin{pmatrix} \mathrm{Re}\,\mathbf{e}_k \\ \mathrm{Im}\,\mathbf{e}_k \\ D_\mathrm{t}\mathrm{Re}\left(\Gamma_\mathrm{t}\mathbf{e}_k\right) \\ D_\mathrm{t}\mathrm{Im}\left(\Gamma_\mathrm{t}\mathbf{e}_k\right) \\ 0 \end{pmatrix}, \tag{30}$$

where we have defined $\mathbf{e}_{1,2,3,4} = \mathbf{E}_1, \mathbf{E}_2, i\mathbf{E}_1, i\mathbf{E}_2$ (again, $\mathbf{E}_{1,2}$ are any two threshold solutions to Eq. (13)). It is shown in Appendix C that the eigenvalue at the next order, $\sigma_{1/2}$ is also zero. Hence, stability is determined by σ_1. At order d, Eq. (25) is

$$(\mathsf{B}_0\sigma_1 + \mathsf{A}_1)\mathsf{x}_0 + \mathsf{A}_{1/2}\mathsf{x}_{1/2} + \mathsf{A}_0\mathsf{x}_1 = 0. \tag{31}$$

Here, all quantities except σ_1 and x_1 are known. Because $\sigma_0 = 0$, we have $\mathsf{A}_0\mathsf{v}_k = 0$. There are also left eigenvectors [32] w_j that satisfy $\mathsf{A}_0^T\mathsf{w}_j = 0$. By acting on Eq. (31) with these left eigenvectors, we obtain a 4×4 *linear* eigenvalue problem for the eigenvalue σ_1 and the eigenvectors (whose elements are the coefficients b_k in Eq. (29)). We can then, in a straightforward fashion, write down the eigenvalues and eigenvectors in closed form. While the procedure we have just described can be done with any basis $\mathbf{E}_{1,2}$, again, it is most convenient to choose the basis $\mathbf{E}_\pm$, due to the symmetry properties which greatly simplify the calculation. Here, we present the results, leaving the detailed derivation to Appendix C.

For the circulating lasing modes in Eq. (18), the four eigenvalues are, in no particular order,

$$\begin{aligned} \sigma_1 &= 0 \\ \sigma_1 &= 2\mathrm{Im}\left(\frac{I}{H}\right)|a|^2 \\ \sigma_1 &= \left(\mathrm{Im}\left(\frac{J}{H}\right) + \sqrt{\left|\frac{K}{H}\right|^2 - \mathrm{Re}\left(\frac{J}{H}\right)^2}\right)|a|^2 \\ \sigma_1 &= \left(\mathrm{Im}\left(\frac{J}{H}\right) - \sqrt{\left|\frac{K}{H}\right|^2 - \mathrm{Re}\left(\frac{J}{H}\right)^2}\right)|a|^2, \end{aligned} \tag{32}$$

where $|a|^2 \equiv \frac{\omega_1 H + G_D}{I}$. The first eigenvalue comes from the global phase degree of freedom for lasing solutions [7]. For the other three eigenvalues, we have found empirically that the real part is always negative, indicating that the circulating modes are stable. Although we have been unable to prove that $\mathrm{Re}(\sigma_1) < 0$ in general for the last three values in Eq. (32), we have empirically observed this to be true, and it is easily checked in any specific case by integrating the threshold modes to compute H, I, J, and K.

For the $n \neq 4\ell$ standing lasing modes in Eq. (19), the eigenvalues are given by

$$\begin{aligned} \sigma_1 &= 0 \\ \sigma_1 &= 0 \\ \sigma_1 &= 2\mathrm{Im}\left(\frac{2I+J}{H}\right)|a|^2 \\ \sigma_1 &= -2\mathrm{Im}\left(\frac{J}{H}\right)|a|^2, \end{aligned} \tag{33}$$

where $|a|^2 \equiv \frac{\omega_1 H + G_D}{2I+J}$. Here, both zero eigenvalues come from continuous degrees of freedom: one comes from the global phase degree of freedom, while the other comes from the relative phase between $\mathbf{E}_+$ and $\mathbf{E}_-$ in Eq. (19), which can take any value (as explained previously, this degree of freedom is likely removed at higher orders in d, so that only certain linear combinations, namely the n-fold rotations of $\mathbf{E}_\mathrm{even}$ and $\mathbf{E}_\mathrm{odd}$, are actually lasing solutions). For TM modes in 2d, which have $\mathbf{E} = E\hat{\mathbf{z}}$ [33], it can be shown that $I = J$, so at least one of the two non-zero eigenvalues here must have a positive real part (in practice, it is always the last eigenvalue), indicating that these standing lasing modes are always unstable. Figure (3) shows a comparison between the theoretical first-order approximation and the exact numerical values of the circulating and standing-wave stability eigenvalues for a $C_{n\mathrm{v}}$ case with $n = 5$.

For the $n = 4\ell$ standing-wave modes, we first have the

$\mathbf{E}_+ \pm \mathbf{E}_-$ solutions in Eq. (20), which have the eigenvalues

$$\begin{aligned}
\sigma_1 &= 0 \\
\sigma_1 &= 2\mathrm{Im}\left(\frac{2I+J+K}{H}\right)|a|^2 \\
\sigma_1 &= \left[-\mathrm{Im}\left(\frac{J+3K}{H}\right)+\rho\right]|a|^2 \\
\sigma_1 &= \left[-\mathrm{Im}\left(\frac{J+3K}{H}\right)-\rho\right]|a|^2 \\
\rho &\equiv \sqrt{\mathrm{Im}\left(\frac{J-K}{H}\right)^2 - 8\mathrm{Re}\left(\frac{K}{H}\right)\mathrm{Re}\left(\frac{J+K}{H}\right)},
\end{aligned} \tag{34}$$

where $|a|^2 \equiv \frac{\omega_1 H + G_D}{2I+J+K}$. Again, there is a zero eigenvalue coming from the global phase degree of freedom. For almost all cases, we have empirically observed that the second eigenvalue has a negative real part, but also $-\mathrm{Im}\left(\frac{J+3K}{H}\right) > 0$, and hence the third and fourth eigenvalues are unstable. However, there are pathological cases where the gain profile $D_0(\mathbf{x})$ can be chosen (e.g., in terms of 4ℓ delta functions) so that $J = -K$, upon which the third eigenvalue is stable, and the last eigenvalue is zero. This zero eigenvalue turns out to become positive (unstable) for physical, finite-sized gain regions, as discussed further in Appendix. C.

Finally, we have the $\mathbf{E}_+ \pm i\mathbf{E}_-$ solutions for the $n = 4\ell$ case in Eq. (21). The eigenvalues are

$$\begin{aligned}
\sigma_1 &= 0 \\
\sigma_1 &= 2\mathrm{Im}\left(\frac{2I+J-K}{H}\right)|a|^2 \\
\sigma_1 &= \left[\mathrm{Im}\left(\frac{3K-J}{H}\right)+\eta\right]|a|^2 \\
\sigma_1 &= \left[\mathrm{Im}\left(\frac{3K-J}{H}\right)-\eta\right]|a|^2 \\
\eta &\equiv \sqrt{\mathrm{Im}\left(\frac{J+K}{H}\right)^2 + 8\mathrm{Re}\left(\frac{K}{H}\right)\mathrm{Re}\left(\frac{J-K}{H}\right)},
\end{aligned} \tag{35}$$

where $|a|^2 \equiv \frac{\omega_1 H + G_D}{2I+J-K}$. Again, in most cases we have empirically found that the second eigenvalue is stable while the third and fourth are unstable. However, there are pathological delta-function cases where the external pump profile $D_0(\mathbf{x})$ can be chosen in a specific way (different from that for the $\mathbf{E}_+ \pm \mathbf{E}_-$ solutions) such that $J = K$, and the third eigenvalue is stable while the fourth is zero. Again, this zero eigenvalue becomes positive (unstable) for finite-size gain regions, and so this marginal case is unlikely to be of practical importance.

We note that the absence of a positive value for σ_1 for the circulating lasing mode does not guarantee that the true eigenvalue σ (Eq. (28)) will remain below the real axis for all d. Indeed, Ref. [7] (Fig. 1 in the reference) found an instance of a 1d uniform ring laser where, for certain regimes, the circulating mode actually becomes unstable above a certain d_{cutoff}. The instability comes

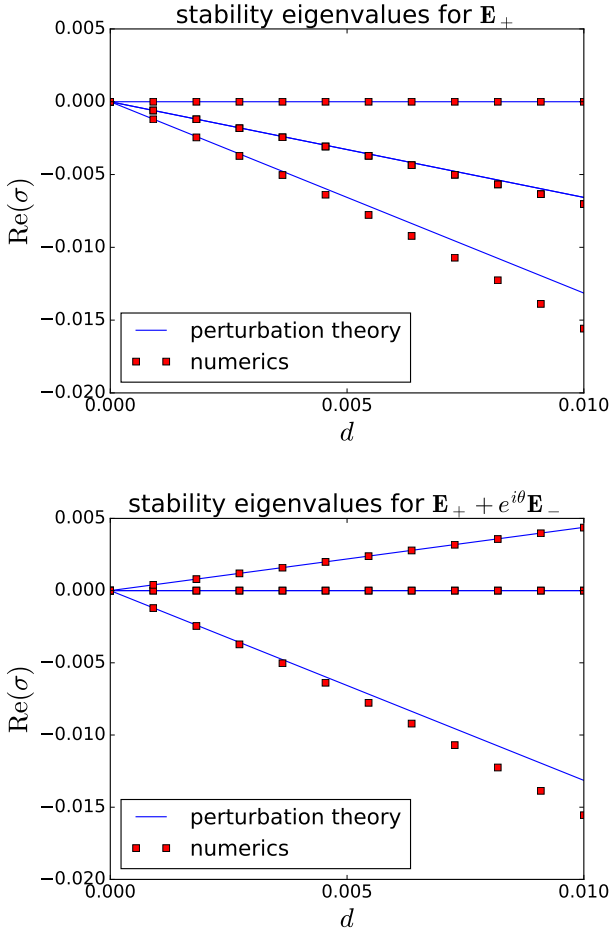

Figure 3. (Color online) Stability eigenvalues for the circulating (top) and standing (bottom) lasing modes from Fig. (2). For each lasing mode, the four lowest eigenvalues obtained using the numerical procedure of Ref. [7] are matched against the four eigenvalues found in perturbation theory. In the top panel, a zero eigenvalue is clearly seen, coming from the global phase freedom. The real parts of the third and fourth values of Eq. (32) are equal, so two of the curves coincide. None of the other eigenvalues go above the real axis, indicating that the circulating mode is stable. For the bottom panel, there are two zero eigenvalues, in agreement with Eq. (33). One of the other two eigenvalues becomes positive, indicating that the standing lasing mode is not stable.

from one of the four Maxwell–Bloch stability eigenvalues associated with the degenerate threshold pair (whose first-order coefficients are given in Eq. (32)) going above the real axis. However, the onset of the instability depends on the value of $\gamma_\parallel$, the relaxation rate of the inversion, and the eigenvalues in Eq. (32) are independent of that parameter, so the effect must come from higher orders. Closer inspection of the data in the ring laser of Ref. [7] shows that for very small $\gamma_\parallel$, the cutoff pump strength d_{cutoff} is linear with $\gamma_\parallel$; that is, the circulating mode is stable for $d < z_0\gamma_\parallel$, where z_0 is a constant independent of d and $\gamma_\parallel$. In Appendix C, we rigorously

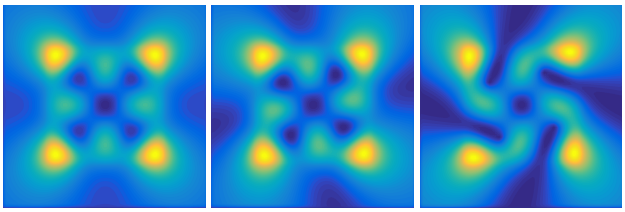

Figure 4. (Color online) The incorrect (left) intensity pattern, correct (center) intensity pattern for the pair of low-Q dielectric square modes, slightly above threshold (the pattern remains essentially the same even for much higher pump strengths), and degenerate passive mode of opposite chirality (right) of low-Q dielectric square for lasing very high above threshold ($D_0 = 100D_t$). The left intensity pattern was obtained by solving two-mode SALT without any interference effects, while the center pattern was obtained by constructing the stable linear combination predicted by symmetry and perturbation theory and then solving single-mode SALT. The correct pattern clearly has a chirality, which the incorrect pattern lacks. The profile on the right is not simply a mirror flip of the lasing mode, but is in fact degenerate with it, as explained in Appendix B.

explain this criterion by extending the perturbation theory used to obtain σ_1 and finding the $\gamma_{\|}$ dependence to all orders in d (Eq. (C50)).

C. Threshold perturbation examples

Now, we illustrate the ideas of threshold perturbation theory with an example of a symmetric geometry with degeneracies: a dielectric square. Unlike in a metal square (with Dirichlet boundary conditions), the equation for the electric field is not separable in the x and y directions. The modes $\mathbf{E}_1$ and $\mathbf{E}_2$ are shown in the middle panel of Fig. (1). The stable linear combination is the circulating mode predicted by Sec. III B. As a consequence of including interference between the two standing-wave modes $\mathbf{E}_{\rm even}$ and $\mathbf{E}_{\rm odd}$, this intensity pattern $|\mathbf{E}_{\rm even} \pm i\mathbf{E}_{\rm odd}|$ is chiral (with C_4 symmetry) while a naive summation of the individual intensities $|\mathbf{E}_{\rm even}|^2 + |\mathbf{E}_{\rm odd}|^2$ would still yield a C_{4v} pattern, as shown in Fig. (4). Because C_n symmetry groups have no 2d irreps, one would normally not expect there to be a degeneracy. However, a key point is that the degeneracy indeed persists even when C_{nv} symmetry becomes C_n, as a consequence of electromagnetic reciprocity [13], as explained in Appendix B. Since this degeneracy does not come from geometric symmetry alone, there is no simple symmetry operation that takes the lasing mode (center panel of Fig. (4)) to its degenerate partner (right panel), e.g., they are not mirror flips. However, there is still an exact degeneracy.

IV. EFFECTS OF CHIRALITY

In this section, we discuss the effects of chirality. So far, we have worked with C_{nv} geometries, which are symmetric under n-fold rotations and flip operations across the mirror planes [5, 21]. However, if the mirror symmetry is broken, then we no longer have C_{nv} symmetry: while there is still symmetry under n-fold rotations, the geometry aquires a certain "handedness", as in the last two panels of Fig. (4). These symmetry groups are known as C_n, and have different consquences for lasing modes arising from these geometries, as we discuss below.

There are two ways for mirror symmetry to be broken: first, for a C_{nv}-symmetric geometry [dielectric function $\varepsilon(\mathbf{x})$ and gain profile $D_0(\mathbf{x})$], the intensity patterns of the circulating modes (given in Eq. (16), and which we have observed are always the only stable modes) turn out to have C_n symmetry as opposed to C_{nv} symmetry, leading to spontaneous breaking of mirror symmetry as soon as the mode starts lasing (the only exception to this rule is for a $C_{\infty v}$ system, in which the circulating lasing modes have an intensity pattern $|\mathbf{E}|^2 \propto |e^{i\ell\phi}|^2 = 1$, and hence still have mirror symmetry). We have also observed that circulating lasing modes in *lossy* C_{nv}-symmetric cavities (such as that in Fig. (4)), those with low quality factor [33] $Q \equiv -\mathrm{Re}\,\omega'/\mathrm{Im}\,\omega'$, where ω' is the passive [zero pump] pole in the Green's function, tend to have greater chirality than circulating modes in cavities with *high* Q (such as that in Fig. (12)). Second, the geometry itself can already have C_n symmetry, e.g., the dielectric and gain functions themselves have chirality. Whether the chirality is due to the intensity pattern of a lasing mode or due to the geometry itself, the effects are similar.

First, the presence of chirality affects the nature of the degeneracy between the lasing mode and its passive pole, e.g., the solution to Eq. (6). For a laser with C_{nv} symmetry at threshold, the two chiral circulating modes, Eq. (16) are exactly related to each other by a mirror-flip operation. As soon as $\mathbf{E}_+$ starts lasing, the mirror symmetry is broken (for $n \neq \infty$) and the passive pole, which we denote as $\tilde{\mathbf{E}}_-$, will move further and further away from being the mirror flip of $\mathbf{E}_+$ (as seen in the right panel of Fig. (4)). It is important to note that if $\mathbf{E}_-$ were to lase instead of $\mathbf{E}_+$, then the *lasing* mode $\mathbf{E}_-$ will be an exact mirror flip of $\mathbf{E}_+$, while the eigenfunction of its passive pole $\tilde{\mathbf{E}}_+$ will be an exact mirror flip of $\tilde{\mathbf{E}}_-$, due to the C_{nv} symmetry at threshold. The lasing frequency ω will also be independent of whether $\mathbf{E}_+$ or $\mathbf{E}_-$ lases, as confirmed by Eq. (18). On the other hand, if the laser already had C_n symmetry at threshold (either due to chirality in a previously lasing mode or in the dielectric or gain functions), then the threshold eigenfunctions $\mathbf{E}_\pm$ are no longer mirror flips of each other, even though their threshold frequencies are both the same ω_t (as an interesting consequence of Lorentz reciprocity of Maxwell's equations, as reviewed in Appendix. A). The fact that $\mathbf{E}_+$ and $\mathbf{E}_-$ are not mirror flips of each other causes a splitting between the overlap integrals I_+ and

I_-, as well as in $J_\pm$ and $H_\pm$. As a consequence, the expressions for the amplitude $|a|$ and the frequency shift ω_1 in Eq. (18) will have I_+ if $\mathbf{E}_+$ lases, and I_- if $\mathbf{E}_-$ lases. Hence, if the symmetry is only C_n at threshold, the clockwise and counterclockwise lasing modes would also have different amplitudes and frequencies, in addition to not being related to each other by a mirror flip operation. These facts allow us to imagine a situation in which there is a "binary tree" of allowed possibilities, e.g., the first degenerate pair lases in clockwise mode, the second in counterclockwise, and so on, and each branch of the tree has distinct lasing amplitudes and frequencies.

Second, the presence of chirality affects the perturbation theory results for standing-mode lasing solutions in Sec. III. When the threshold symmetry is C_{nv}, there exist standing-mode solutions of the form $\mathbf{E} \propto \mathbf{E}_+ + e^{i\theta}\mathbf{E}_-$ (Eq. (19)) when $n \neq 4\ell$, and standing-wave modes of the form $\mathbf{E} \propto \mathbf{E}_+ \pm \mathbf{E}_-$ and $\mathbf{E}_+ \pm i\mathbf{E}_-$ when $n = 4\ell$. However, when the threshold symmetry is C_n, there are no longer any standing-mode lasing solutions for the $n \neq 4\ell$ case. In the $n = 4\ell$ case, however, we have found empirically that the standing-mode solutions $\mathbf{E}_+ \pm \mathbf{E}_-$ and $\mathbf{E}_+ \pm i\mathbf{E}_-$ still exist (provided that the correct normalization and overall phase of $\mathbf{E}_-$ is chosen appropriately). However, because of the splitting in the values of the overlap integrals $I_\pm$, $J_\pm$, and $K_\pm$ for the C_n case, the stability eigenvalues (Sec. III B) for these standing-mode solutions will no longer be given by the simple expressions in Eq. (34) and Eq. (35), and will have to be numerically computed (nevertheless, we have empirically found that these standing-mode solutions are still unstable).

A. Multimode lasing

So far, the discussion and examples in this paper have dealt with the case in which only one pair of degenerate modes are lasing. The generalization to the case of multimode lasing (i.e. multiple nondegenerate and degenerate lasing modes all lasing simultaneously) is straightforward. Since our method combines degenerate pairs into a single mode that is the stable linear combination (as given by the perturbation theory in Sec. III, the multimode treatment is exactly the same as for SALT without degeneracies: the degenerate pairs are always treated as a single mode. As in previous work on SALT [8, 12, 14], all lasing modes are solved simultaneously at first, and there the collective effect of their spatial hole-burning is used to track the passive modes and add any mode (degenerate or nondegenerate) that crosses threshold to the list of lasing modes. The only aspects of our method requiring generalization are the threshold perturbation theory of Sec. III and the *quadratic program* [34] (QP) method of Sec. V A. For both aspects, we describe small tweaks to the methods presented in those sections that make them valid for the case of multimode lasing.

A general situation in which multimode-lasing is occuring can be described by Eq. (4) [8, 12], where there are M lasing modes ($\mu = 1, 2, \ldots, M$). If we start with C_{nv} symmetry and have lasing modes that are either circulating modes (as in Sec. III B) or non-degenerate modes (partners of *real* 1d irreps without a corresponding complex-conjugate irrep of the opposite chirality), then each of the $|\mathbf{E}_\nu|^2$ terms has at least C_n symmetry, so the full stationary inversion $D(\mathbf{x})$, which includes the effects of spatial hole-burning, has C_n symmetry. Suppose that the pump strength is at the threshold of mode M so that this mode has just started lasing, and that only modes 1 through $M-1$ contribute to the spatial hole-burning. Then all results in Sec. III still hold, except with gain profile $D_0(\mathbf{x})$ replaced by $D(\mathbf{x})$. While the gain profile is now C_n symmetric rather than C_{nv}, the presence of chiral degenerate pairs (which requires only C_n symmetry and Lorentz reciprocity, as explained in Appendix B) still remains, as explained in Sec. III B (the arguments in that section do not assume C_{nv} symmetry, so they still hold even if $D_0(\mathbf{x})$ is replaced by a function with only C_n symmetry.

V. C_{nv} SYMMETRY BROKEN BY DISCRETIZATION

In many cases, the C_{nv}-symmetric geometry we are trying to solve has a degeneracy that is broken when the geometry is approximated by a discretized grid for numerical solution on a computer [14, 35, 36], since the grid may no longer have the original C_{nv} symmetry. For linear equations, this unphysical splitting is not an issue because it is usually straightforward to tell whether a pair of modes is "really" degenerate by how it corresponds to the eigenfunctions of the "real" symmetry group, and since all linear superpositions solve the equation in the infinite-resolution limit, we can construct arbitrary superpositions as needed *after* solving for both of the modes. However, for SALT (which is nonlinear), the coefficients of the superposition are physical quantities that must be found by our solution method, as explained in Sec. III B. As explained in Ref. [14], the process for solving for lasing modes begins with the linear problem for the passive poles. Because both the real and imaginary parts of the passive poles are split by the discretization error, the modes will lase at different pump strengths, and even after both modes lase we cannot construct a linear combination of them because the two modes satisfy equations with different real eigenfrequencies.

When the pump strength is sufficiently high above threshold, however, the two near-degenerate modes can interact with each other via the nonlinear spatial hole burning interaction to form a single stable laser mode. This effect is commonly known as cooperative frequency locking [19, 20]. For example, Ref. [7] found instances where intentionally breaking a degeneracy, such as by introducing a wedge at a single location on the rim of a ring laser, can result in the circulating mode not existing near threshold as expected, but coming back *into* existence

(once the pump strength is high enough above threshold and the nonlinearity is strong enough) as a modified version that is nearly the degenerate circulating mode. We have found similar results in hexagonal (C_{6v}) structures *without* artifically-introduced defects, in which the degeneracy is broken by discretization alone. There, a circulating single-mode lasing solution starts existing above a certain pump strength (somewhat higher than threshold), even though there is no degeneracy at threshold. The reason the circulating lasing mode requires a minimum pump strength is that the nonlinearity must be strong enough to counteract the broken degeneracy and to lock the two modes to a single frequency. In many cases such as these, numerically solving the single mode problem, using an artificially-constructed circulating solution as an initial guess, results in the solver correctly converging to a circulating lasing mode. However, this effect is not yet completely understood, and it is not entirely predictable under what circumstances such a circulating mode exists. Furthermore, the pump window between the original lasing threshold and the threshold at which the stable circular mode emerges can not be described with SALT as the electric field no longer shows a multi-periodic time dependency [19, 20]. Moreover, a discretization-induced error and a physical perturbation breaking the degeneracy are two distinct effects (even if their consequences are mathematically similar), and it is useful to be able to study them independently. When one is studying a physical symmetry-breaking defect, one does not want to accidentally observe an artificial effect of discretization instead. To eliminate numerical symmetry breaking at arbitrary pump strengths, we therefore devised a solution: we construct a minimal perturbation to the dielectric function that restores the degeneracy in both the pump strengths and the frequencies at threshold. We discuss this method below.

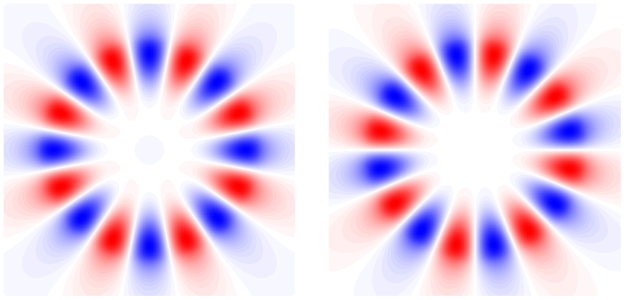

Figure 5. (Color online) $\ell = 8$ threshold modes [$\mathrm{Re}(\mathbf{E}_{e,o})$] for a cylinder with uniform dielectric $\varepsilon = 5$ and radius $r = 1$. Unlike in the odd-ℓ case (Fig. (1)), however, the discretized modes are *not* $\frac{\pi}{2}$ rotations from each other. Consequently, there is an unphysical splitting, due to discretization, of 0.11% in $\mathrm{Re}(\omega_1 - \omega_2)$ (for a resolution of 14 pixcels per wavelength) and 11.5% in $\mathrm{Im}(\omega_1 - \omega_2)$ at zero pump strength (the latter being larger only because these are high-Q modes and $\mathrm{Im}(\omega_\mu)$ is already very small at zero pump strength). A difference in imaginary parts also means a splitting in the threshold pump strength D_t.

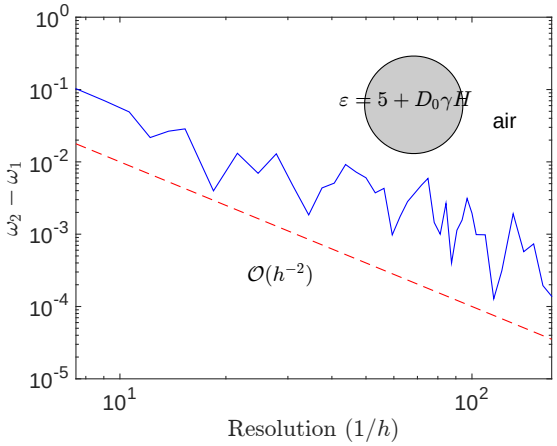

Figure 6. (Color online) Splitting in degeneracy due to discretization error for even-ℓ modes of dielectric cylinder versus the resolution $1/h$ of the discretization, where h is the distance between adjacent gridpoints. The oscillations, which are due to the discontinuous interfaces between dielectric and air that "jump" when the resolution is changed, could in principle be smoothed by using subpixel averaging techniques for the discretization [37].

A. Restoring degeneracy by minimal perturbations

The basic idea is that we construct an artificial perturbation $\delta\varepsilon(\mathbf{x})$ to the dielectric permittivity that forces the degeneracy in both the frequency and threshold, and then we solve the perturbed single-mode SALT equation. There are infinitely many possible functions that can achieve this goal, so we look for the one with the smallest L_2 norm $\|\delta\varepsilon(\mathbf{x})\|_2^2 = \int |\delta\varepsilon(\mathbf{x})|^2$. This is a good choice because in the limit of infinite resolution, the perturbation $\delta\varepsilon(\mathbf{x})$ approaches zero. We construct $\delta\varepsilon(\mathbf{x})$ by solving a *quadratic program* [34] (QP) with linear constraints that we obtain using perturbation theory. Not only does this uniquely (and cheaply) determine $\delta\varepsilon$, as described below, but it also guarantees convergence to the solution of the unperturbed (physical) single-mode SALT equation in the limit of infinite resolution. The reason it guarantees convergence is that the frequency splitting vanishes in the limit of infinite resolution, as shown in Fig. (6), and so the minimum-norm $\delta\varepsilon$ to force a degeneracy also vanishes in the limit of infinite resolution, recovering the unperturbed SALT.

It turns out that determining the minimum-norm $\delta\varepsilon$ requires only that we solve a sequence of QP problems: minimizing a convex quadratic function ($\|\delta\varepsilon\|_2^2$) of $\delta\varepsilon$ subject to a linear constraint on $\delta\varepsilon$. QPs are convex optimization problems with a unique global minimum that can be efficiently found simply by solving a system of

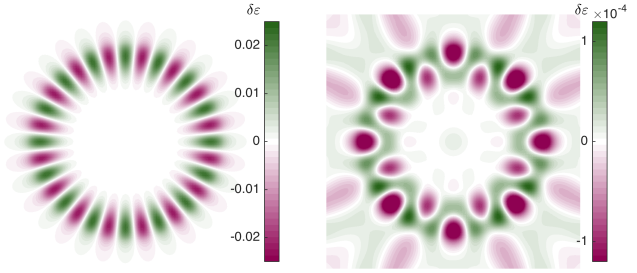

Figure 7. (Color online) Dielectric perturbation $\delta\varepsilon$ obtained by solving QP for threshold modes with $\ell = 8$. The real part (left) has a dependence $\cos(2\ell\phi)$, while the imaginary part (right) is a more complicated function.

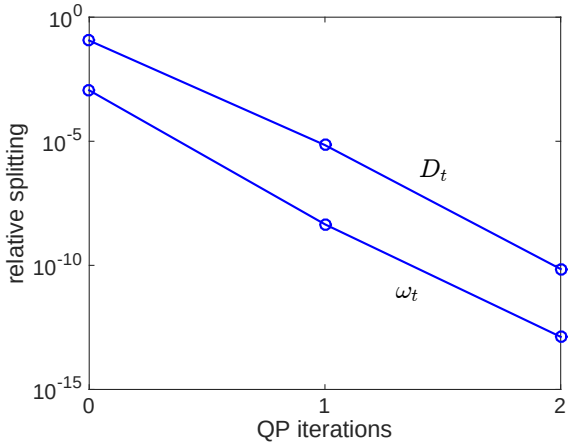

Figure 8. (Color online) Relative splitting in threshold pump strength D_t and frequency ω_t for even-ℓ cylinder modes after QP iterations. The relative splitting in frequency is defined in the usual way as $2\left|\frac{\omega_1-\omega_2}{\omega_1+\omega_2}\right|$, and similarly for the pump strength. Only two iterations of QP were required reduce the splitting in both the threshold frequency ω_t and the threshold pump strength D_t to 10^{-10} or smaller.

linear equations [34]. In particular, the linear constraint (Eq. (D7)), which coalesces the eigenvalues, can be derived from perturbation theory. Because the perturbation theory is only first-order, however, the $\delta\varepsilon$ that we find by solving the QP only approximately eliminates the splitting, but we can simply re-solve SALT and solve a new QP, iterating the process a few times (twice is typically enough) to force a degeneracy to machine precision. The full details of the procedure are given in Appendix D.

The resulting $\delta\varepsilon$ of this procedure applied to the even-ℓ threshold modes in Fig. (5) is shown in Fig. (7), and the convergence of the splitting to zero is shown in Fig. (8). As verified in Fig. (9), the L_2 norm of $\delta\varepsilon(\mathbf{x})$ decreases with resolution, satisfying our requirement that the dielectric perturbation should go to zero in the continuum limit. In principle, one must resolve for $\delta\varepsilon$ at each pump strength, since the hole-burning term changes the problem. However, in practice we have found changes in $\delta\varepsilon$ with pump strength to be negligible, as in Fig. (10), and one can typically use the same $\delta\varepsilon$ for all pump strengths. In Appendix D, we give a method that re-forces the degeneracy for pump strengths above threshold, if a machine precision degeneracy is desired.

B. Example with C_{6v} symmetry

An example of a hexagonal cavity is shown in Fig. (1). This geometry was adapted from an infinite lattice of period a with air holes of radius $0.3a$. A single hole in the middle has a reduced radius $0.2a$ to create a defect in the band gap. The dielectric is $\varepsilon_c = 11.56$ everywhere except in the holes, where there is air. A perfectly matched layer (PML) is added to the boundaries to simulate the radiation loss, and the axes of the hexagon have been aligned with the diagonals rather than the x and y axes because the finite-difference Yee discretization [36] happens to only have mirror symmetry along the diagonals. Here, the lasing modes are TE (electric field in-plane and magnetic field out of plane), and there is a pair of degenerate threshold modes from the hexagon's C_{6v} symmetry, as shown in Fig. (1). For a 100×100 finite-difference discretization, there is about a 1.5% splitting between the threshold eigenvalues, so again we must use the QP procedure to force the threshold degeneracy. Since these are TE modes, we now have *two* components of the electric field, and consequently we may treat $\delta\varepsilon$ as a tensor, as in Eq. (D4). We only consider the diagonal components $\delta\varepsilon_{xx}$ and $\delta\varepsilon_{yy}$ here for simplicity. Only two iterations of QP are necessary to force the degeneracy down to machine precision, and the perturbation used to force the degeneracy is shown in Fig. (11). We then use Eq. (16) as an initial guess for our numerical solver, and the intensity pattern of the resulting circulating solution is shown in Fig. (12).

C. Multimode case

Now we consider how to treat the problem of discretization-broken symmetry (Sec. V) in the case of multimode lasing. The method of Sec. V A gives a $\delta\varepsilon(\mathbf{x})$ that forces the threshold degeneracy for a *single* mode pair. When there are multiple pairs of nearly degenerate modes the generalization is straightforward: we allow each pair to have its *own* $\delta\varepsilon_\mu$, so that their degeneracies can be forced *independently*. As a result, the dielectric for each pair in Eq. (4) will become

$$\varepsilon_\mu(\mathbf{x}) = \varepsilon(\mathbf{x}) + \delta\varepsilon_\mu(\mathbf{x}) + \frac{D_0(\mathbf{x})\Gamma(\omega_\mu)}{1 + \gamma_\parallel^{-1}\sum|\Gamma_\nu \mathbf{E}_\nu(\mathbf{x})|^2}. \quad (36)$$

Since our QP method finds the $\delta\varepsilon_\mu$ with the lowest L_2 norm (as described in Sec. V A) and the splitting decreases with resolution as seen in Fig. (6), each $\delta\varepsilon_\mu$ will

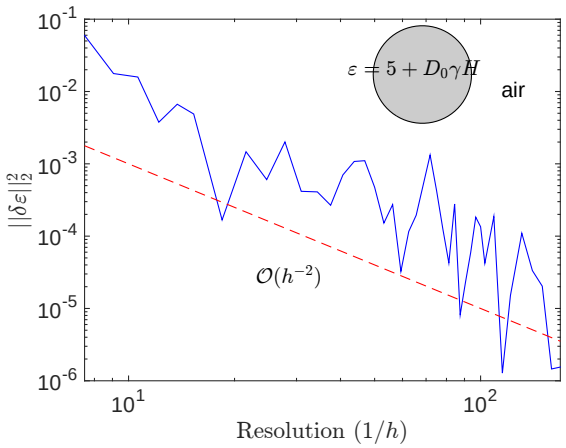

Figure 9. (Color online) L_2 norm of resulting $\delta\varepsilon(\mathbf{x})$ function obtained from QP procedure versus discretization resolution $1/h$ for nearly degenerate even-ℓ modes of the cylinder, where h is the spacing between adjacent gridpoints. The same resolutions as in Fig. (6) were used, and the oscillations resemble the curve for splitting very closely. This is because the larger the splitting $\omega_2 - \omega_1$, the larger the $\delta\varepsilon(\mathbf{x})$ function needed to enforce the degeneracy. The fact that $\|\delta\varepsilon\|_2^2$ appears to be going to zero as the resolution increases indicates that our QP procedure is convergent.

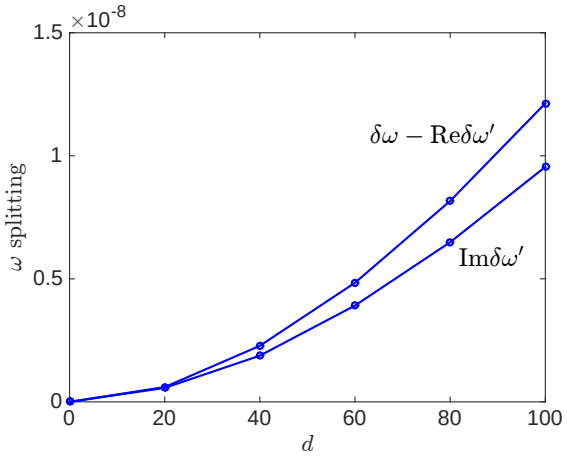

Figure 10. (Color online) Above-threshold splitting in real and imaginary parts of $\delta\omega'$ after performing QP procedure for even-ℓ modes. The magnitude is very small because the intensity profile is very close to rotationally symmetric.

independently go to zero as we increase the resolution, so this generalized method is also *convergent*: the unphysical frequency-dependent $\delta\varepsilon_\mu$ vanishes with increasing resolution.

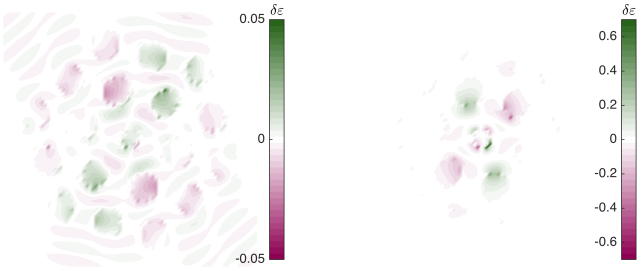

Figure 11. (Color online) Dielectric perturbation obtained from QP procedure for hexagonal cavity. Since the mode is TE ($\mathbf{E} = E_{\mathrm{even}}\hat{\mathbf{x}} + E_{\mathrm{odd}}\hat{\mathbf{y}}$), we have allowed the perturbation to be a diagonally-anisotropic tensor, as in Eq. (D4). Shown here are the real (left) and imaginary (right) parts of $\delta\varepsilon_{xx}$. The $\delta\varepsilon_{yy}$ looks similar except rotated by 60 degrees.

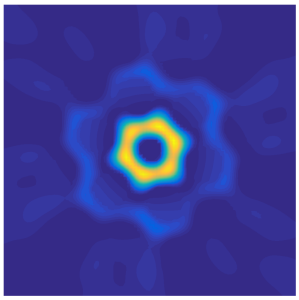

Figure 12. (Color online) Intensity pattern for stable lasing mode for hexagonal cavity. The pattern appears to be six-fold symmetric, which is expected. Unlike in the right panel of Fig. (4) however, the chirality is not significant enough to be visible, since the hexagonal cavity is not as lossy as the square cavity in Fig. (4). In the ideal system, the second pole $\delta\omega'$ stays degenerate with the lasing eigenvalue $\delta\omega$, and this linear combination stays stable for all pump strengths above threshold. In the discretized system, there is not a true $C_{6\mathrm{v}}$ symmetry, so there is a small splitting similar to that of the even-ℓ cylinder modes. Again, this splitting is too small to affect physically meaningful results of the simulation, but can be removed using the QP procedure if desired.

VI. CONCLUDING REMARKS

In this paper, we have reduced the problem of identifying the stable lasing modes of a degenerate laser from the full nonlinear Maxwell–Bloch equations to a small *semi-analytical* solution evaluated in terms of integrals of the threshold modes (solutions to the *linear* Maxwell partial-differential equation). Our perturbative solution near threshold confirms an ansatz in the earlier degenerate SALT work [7], in which the circulating and standing wave solutions were guessed as starting points for a SALT solver and it was conjectured that the resulting four solutions were the only possibilities. Furthermore, we have presented an efficient numerical scheme to track these solutions far above threshold via numerical SALT solvers [14] combined with a simple technique to correct for numerical symmetry breaking. And finally, we have shown

that the degeneracy of the C_n group Sec. IV means that circulating lasing modes will retain a degenerate passive pole even far above threshold, where the hole-burning term breaks mirror symmetry. In addition, our work poses some intriguing open questions for future research.

First, although we have reduced the question of stability of circulating modes near threshold to a simple semi-analytical criterion (checking whether a certain integral expression is positive), one would like to additionally have a fully analytical proof that the circulating modes are stable, or alternatively a counter-example of a $C_{n\mathrm{v}}$-symmetric problem with a degenerate lasing threshold in which the circulating mode is unstable. Since Ref. [7] found that circulating modes can become unstable at higher pump strengths, one might naively hope that the technique of Ref. [38] (in which a lasing SALT solution at some pump strength above threshold is transformed into a threshold SALT solution by designing the pump profile at threshold to match the hole-burning term at the higher pump strength) could be used to translate these into an unstable threshold circulating mode. However, the technique of Ref. [38] only translates one SALT solution into another, and does not translate the full Maxwell–Bloch solutions since it does not keep track of $\gamma_\parallel$. Because the exact Maxwell–Bloch stability eigenvalue σ depends on $\gamma_\parallel$, as explained in Appendix C 4 (only the first-order term σ_1 is independent), and SALT solutions do not, this method of translating a hole-burning term to an artificially-designed pump profile at a higher threshold does not account for the effects of $\gamma_\parallel$.

Second, it would be interesting to extend this sort of perturbative SALT/stability analysis to other lasing systems besides C_n and $C_{n\mathrm{v}}$ symmetries. For example, in a 3d photonic-crystal cavity [33] one could have cubic symmetry and threefold degeneracies, or one could have even greater degeneracies in spherical resonators. Alternatively, in a surface-emitting distributed feedback [39–42] or photonic-crystal laser [43–46], one might have lasing occur at a "band edge" [47] in the dispersion relation. While a band edge may or may not be degenerate *per se*, it coincides with a singularity in the density of states [48] where a continuum of resonances occurs in a small neighborhood of the lasing resonance, and perturbative analysis might be very helpful in understanding its stability. Finally, it would be interesting to apply semi-analytical perturbative stability analysis to cases where a small imperfection slightly splits the degeneracy, which was studied numerically in Ref. [7].

ACKNOWLEDGMENTS

This work was supported in part by the Army Research Office through the Institute for Soldier Nanotechnologies (ISN), Grant No. W911NF-07-D-0004, the Air Force Research Laboratory under agreement number FA8650-15- 2-5220, and by the Austrian Science Fund (FWF) through Project No. SFB NextLite F49-P10. L. G. acknowledges partial support by NSF under Grant No. DMR-1506987. We are also grateful to A. D. Stone for helpful discussions. The U.S. Government is authorized to reproduce and distribute reprints for governmental purposes notwithstanding any copyright notation thereon. The views and conclusions contained herein are those of the authors and should not be interpreted as necessarily representing the official policies or endorsements, either expressed or implied, of Air Force Research Laboratory or the U.S. Government.

Appendix A: Degeneracy in C_n

We review the result, given in Ref. [13], of the fact that there are two-fold degeneracies (due to Lorentz reciprocity) in geometries with C_n but not $C_{n\mathrm{v}}$ symmetry, even though there are only one-dimensional irreps. We give a slightly simpler and more general proof by exploiting the differential form of Maxwell's equations, as opposed to the integral form in Ref. [13].

Consider a field $\mathbf{E}^+$ that satisfies the equation $\hat{L}(\omega^+)\mathbf{E}^+ = 0$, where we define the linear operator (as in Ref. [49])

$$\hat{L}(\omega) \equiv -\nabla \times \frac{1}{\mu(\mathbf{x},\omega)}\nabla \times + \omega^2\varepsilon(\mathbf{x},\omega) \tag{A1}$$

where ω is the eigenfrequency and ε and μ have C_n symmetry: that is, $R_n\varepsilon R_n^{-1} = \varepsilon$, where R_n is an n-fold rotation and $R_n^n = 1$, the identity operator. Suppose that the field transforms like one of the chiral irreps of C_n: that is, $R_n\mathbf{E}^+ = \exp\left(-\frac{2\pi i m}{n}\right)\mathbf{E}^+$, with $0 < |m| \le \mathrm{floor}(\frac{n-1}{2})$. We want to show that there exists some other function $\mathbf{E}^-$ that transforms according to the irrep of the opposite chirality *and* has the same eigenfrequency: that is, $R_n\mathbf{E}^- = \exp\left(\frac{2\pi i m}{n}\right)\mathbf{E}^-$ and $\hat{L}(\omega^+)\mathbf{E}^- = 0$.

The key step is to use the right basis: we *could* find the Maxwell eigenfrequencies (Green's-function poles) by solving the nonlinear (in ω) eigenvalue problem $\hat{L}(\omega)\mathbf{E} = 0$. However, these make a poor basis because they diagonalize *different* operators $\hat{L}(\omega)$ with $\omega \neq \omega^+$. Instead, we fix $\omega = \omega^+$ and examine the set of eigenfunctions $\mathbf{E}_j^-$ that satisfy $\hat{L}(\omega^+)\mathbf{E}_j^- = \lambda_j\mathbf{E}_j^-$ and that transform as the $\exp\left(\frac{2\pi i m}{n}\right)$ irrep. A similar strategy was employed in Ref. [12] to introduce the threshold constant-flux (TCF) states basis. (The TCF approach is slightly different, for it assumes that the eigenvalues λ_j are followed by a spatial function that specifies the pump profile.) Note that λ_j are *not* squared eigenfrequencies and $\mathbf{E}_j^-$ are *not* Maxwell solutions, except for $\lambda_j = 0$. Because this set is a complete basis for functions of this chirality, the function $(\mathbf{E}^+)^\star$ (which transforms in the same way as $\mathbf{E}_j^-$ because the rotation operator R_n is real) can be expanded in this basis:

$$\left(\mathbf{E}^+\right)^\star = \sum b_j\mathbf{E}_j^-, \tag{A2}$$

assuming that $\hat{L}(\omega^+)$ is diagonalizable (which is generically true for matrices except at exceptional points; the

situation for infinite-dimensional operators is more complicated, but diagonalizability is typically assumed there too in physics). We will now show that at least *one* of these $\mathbf{E}_j^-$ is exactly the $\mathbf{E}^-$ satisfying $\hat{L}(\omega^+)\mathbf{E}^- = 0$ that we are looking for.

First, we define the *unconjugated* inner product $(\mathbf{f}, \mathbf{g}) \equiv \int d^3x\, \mathbf{f} \cdot \mathbf{g}$. Then, for appropriate boundary conditions, $\hat{L}(\omega^+)$ is complex symmetric, that is: $\left(\mathbf{f}, \hat{L}\mathbf{g}\right) = \left(\hat{L}\mathbf{f}, \mathbf{g}\right)$ for reciprocal materials $\varepsilon = \varepsilon^T$, $\mu = \mu^T$, and this is known as Lorentz reciprocity [33]. Because $\hat{L}(\omega^+)$ is complex symmetric, its eigenfunctions with distinct eigenvalues are orthogonal; that is: $\left(\mathbf{E}_i^-, \mathbf{E}_j^-\right) = 0$ for $\lambda_i \neq \lambda_j$. Now write

$$\int d^3x\, \left|\mathbf{E}^+\right|^2 = \sum b_j \left(\mathbf{E}^+, \mathbf{E}_j^-\right). \tag{A3}$$

If all $\mathbf{E}_j^-$ had $\lambda_j \neq 0$, then $\left(\mathbf{E}^+ \cdot \mathbf{E}_j^-\right) = 0$ for all j. However, the left-hand side is obviously positive, so at least one term in the sum on the right-hand side must be non-vanishing. Hence, this term has the eigenvalue $\lambda_j = 0$, and it is precisely the $\mathbf{E}^-$ that is degenerate to $\mathbf{E}^+$.

Appendix B: Allowed lasing modes

In this appendix, we show that the only allowed lasing modes for $C_{n\mathrm{v}}$ geometries above threshold are the circulating modes $\mathbf{E}_\pm$ and standing-wave modes $\mathbf{E}_+ + e^{i\theta}\mathbf{E}_-$, with θ an arbitrary angle for $n \neq 4\ell$ (where ℓ is the order of the 2d irrep that the degenerate modes transform as), and θ an integer multiple of $\frac{\pi}{2}$ for $n = 4\ell$. We begin by writing $D_0 = D_\mathrm{t}(1+d)$ and inserting into Eq. (12). We expand to lowest order in d and the mode intensity, and we have

$$\nabla\times\nabla\times\mathbf{E} = \omega^2\left[\varepsilon + D_\mathrm{t}\Gamma\left(1 + d - \gamma_\parallel^{-1}\left|\Gamma\mathbf{E}\right|^2\right)\right]\mathbf{E}. \tag{B1}$$

Comparing with Eq. (13) at threshold, we conclude that $\mathbf{E} = \mathcal{O}(\sqrt{d})$, and that the profile should be some linear combination of the threshold modes $\mathbf{E}_{1,2}$, as in Eq. (14). Inserting Eq. (14) into Eq. (B1), noting that the zeroth-order terms vanish due to Eq. (13), we obtain

$$\begin{aligned}&\left[\nabla\times\nabla\times - \omega_\mathrm{t}^2\left(\varepsilon + D_\mathrm{t}\Gamma_\mathrm{t}\right)\right]\delta\mathbf{E}\\ &= \left\{\omega_1\frac{\partial}{\partial\omega_\mathrm{t}}\left[\omega_\mathrm{t}^2\left(\varepsilon + D_\mathrm{t}\Gamma_\mathrm{t}\right)\right] + \omega_\mathrm{t}^2 D_\mathrm{t}\Gamma_\mathrm{t}\left(1 - |\mathbf{f}|^2\right)\right\}\mathbf{f}\end{aligned} \tag{B2}$$

where $\mathbf{f} \equiv a_1\mathbf{E}_1 + a_2\mathbf{E}_2$. Now multiply by $\mathbf{E}_{1,2}$ and integrate over all space, and we obtain Eq. (15), where we have used the fact that

$$\int d^3x\, \mathbf{E}_{1,2}\cdot\left[\nabla\times\nabla\times - \omega_\mathrm{t}^2\left(\varepsilon + D_\mathrm{t}\Gamma_\mathrm{t}\right)\right]\delta\mathbf{E} = 0 \tag{B3}$$

because the threshold Maxwell operator is complex-symmetric [33, 50, 51] so that it acts to the left and annihilates $\mathbf{E}_{1,2}$. (The fact that the $\nabla\times\nabla\times$ operator acts to the left can be understood using integration by parts, with the boundary terms vanishing due to the limiting-absorption principle [52].) Now, choose $\mathbf{E}_1 = \mathbf{E}_+$ and $\mathbf{E}_2 = \mathbf{E}_-$, where $\mathbf{E}_\pm$ is defined in Eq. (16). For generality, we assume that the geometry [i.e. the functions $\varepsilon(\mathbf{x})$ and $D_\mathrm{t}(\mathbf{x})$] has at least C_n symmetry. In Eq. (15), we see that $\int d^3x\varepsilon(\mathbf{x})\mathbf{E}_+\cdot\mathbf{E}_+$ vanishes, because it is the conjugated inner product of $\mathbf{E}_+$ and $\mathbf{E}_+^\star$, which transform as the clockwise and counterclockwise 1d irreps in the C_n group, and from the great orthogonality theorem [5, 21], conjugated inner products between functions belonging to different irreps always vanish [e.g., for circulating modes on a uniform ring, the integral $\int d\phi\, e^{i\ell\phi}(e^{-i\ell\phi})^\star$ vanishes]. Also, the integral over $D_\mathrm{t}(\mathbf{x})$ is the same, because it also has at least C_n symmetry. Excluding the intensity term in Eq. (15), the rest of the terms become

$$a_\mp\left(\omega_1 H + G_D\right), \tag{B4}$$

where we have defined

$$\begin{aligned}G_\varepsilon &\equiv \int d^3x\, \varepsilon(\mathbf{x})\mathbf{E}_+\cdot\mathbf{E}_-\\ G_D &\equiv \int d^3x\, D_\mathrm{t}(\mathbf{x})\mathbf{E}_+\cdot\mathbf{E}_-.\\ H &\equiv (\omega_\mathrm{t}^2\Gamma_\mathrm{t})^{-1}\frac{\partial}{\partial\omega_\mathrm{t}}\left\{\omega_\mathrm{t}^2\left(G_\varepsilon + G_D\Gamma_\mathrm{t}\right)\right\}.\end{aligned} \tag{B5}$$

For the intensity term, we have $\int d^3x\, D_\mathrm{t}\mathbf{E}_\pm\cdot\mathbf{f}\,|\mathbf{f}|^2$. We note that the quantities $|\mathbf{E}_\pm|^2$ and $\mathbf{E}_+\cdot\mathbf{E}_-$ have C_n symmetry, so by symmetry arguments, the only surviving integrals are

$$\begin{aligned}I_\pm &= \int d^3x\, D_\mathrm{t}\,|\mathbf{E}_\pm|^2\,\mathbf{E}_+\cdot\mathbf{E}_-\\ J_\pm &= \int d^3x\, D_\mathrm{t}(\mathbf{E}_\pm^\star\cdot\mathbf{E}_\mp)\mathbf{E}_\pm\cdot\mathbf{E}_\pm\\ K_\pm &= \int d^3x\, D_\mathrm{t}(\mathbf{E}_\mp^\star\cdot\mathbf{E}_\pm)\mathbf{E}_\pm\cdot\mathbf{E}_\pm.\end{aligned} \tag{B6}$$

Additionally, note that for $C_{n\mathrm{v}}$, we have $I_+ = I_-$, and the same for J and K. Further, for TM modes ($\mathbf{E}_\pm = E_\pm\hat{\mathbf{z}}$), we have $I_\pm = J_\pm$. Finally, $K_\pm$ is only non-vanishing for $n = 4\ell$, since in that special case, $\mathbf{E}_+$ picks up a factor of i under four-fold rotation, as seen in Eq. (16). With these definitions, Eq. (15) straightforwardly reduces to Eq. (17).

To solve for the coefficients $a_\pm$ and the frequency shift ω_1, first consider the case $a_- = 0$. Dividing Eq. (17) (with the bottom sign) by a_+ then yields

$$|a_+|^2 = \frac{\omega_1 H + G_D}{I_+}. \tag{B7}$$

Taking the imaginary part of both sides, and noting that ω_1 is real, we obtain

$$0 = \omega_1\mathrm{Im}\left(\frac{H}{I_+}\right) + \mathrm{Im}\left(\frac{G_D}{I_+}\right), \tag{B8}$$

which leads to the circulating solution. (Eq. (18) holds for $C_{n\mathrm{v}}$; the same expression with I replaced by $I_\pm$ also holds for C_n. In this case $I_+ \neq I_-$, so the two circulating lasing modes will actually have slightly different amplitudes and frequencies.) Note that the fact that $|a_+|^2$ must be a positive number also gives a cutoff condition

$$\mathrm{Re}(G_D/I_\pm) > \frac{\mathrm{Im}\,(G_D/I_\pm)}{\mathrm{Im}\,(H/I_\pm)}\mathrm{Re}(H/I_\pm). \tag{B9}$$

Next, we consider the case that both $a_\pm$ are nonzero. Write $a_\pm = |a_\pm|\, e^{i\theta_\pm}$ and define the relative phase $z = e^{i(\theta_- - \theta_+)}$. Divide Eq. (17) by $a_\mp$, and we obtain

$$|a_\mp|^2 I_\mp + |a_\pm|^2 \left(I_\pm + J_\pm + z^{\mp 2} K_\pm\right) = \omega_1 H + G_D. \tag{B10}$$

Solving this linear equation for the unknowns $|a_\pm|^2$, we obtain

$$|a_\pm|^2 = (\omega_1 H + G_D) T_\pm, \tag{B11}$$

where

$$T_\pm = \frac{J_\mp + z^{\pm 2} K_\mp}{(I_+ + J_+ + z^{-2}K_+)(I_- + J_- + z^2 K_-) - I_+ I_-}. \tag{B12}$$

Again, since $|a_\pm|^2$ and ω_1 are real, we have

$$\omega_1 = -\frac{\mathrm{Im}\,(G_D T_+)}{\mathrm{Im}\,(H T_+)} = -\frac{\mathrm{Im}\,(G_D T_-)}{\mathrm{Im}\,(H T_-)}. \tag{B13}$$

The second equality here is a constraint that must be satisfied. For $C_{n\mathrm{v}}$ with $n \neq 4\ell$, we have $I_+, J_+ = I_-, J_-$ and $K_\pm = 0$ (as explained previously), so $T_+ = T_-$ and the constraint is automatically satisfied, indicating that z is free to have any phase, and yielding the solution in Eq. (19). For C_n with $n \neq 4\ell$, we again have $K_\pm = 0$, but there is no mirror symmetry so $I_+, J_+ \neq I_-, J_-$, and no choice of z will allow Eq. (B13) to be satisfied. Hence, there are no standing lasing modes for this case.

For $C_{n\mathrm{v}}$ with $n = 4\ell$, we again have $I_+, J_+ = I_-, J_-$, but we also have $K_+ = K_- \neq 0$. Hence, for $T_+ = T_-$ to be true, we must have $z^2 = z^{-2} = \pm 1$. Hence, there are two cases, $z = \pm 1$, for which the solution is given in Eq. (20), and $z = \pm i$, for which the solution is given in Eq. (21). For C_n with $n = 4\ell$, we now have $I_+, J_+ \neq I_-, J_-$, and $K_+ \neq K_-$, with both $K_\pm$ nonzero. Empirically, we have found that Eq. (B13) still has solutions (which must obtained by solving the equation numerically) at four allowed phases z, with angles separated by $\frac{\pi}{2}$, just as in the $C_{4\ell\mathrm{v}}$ case. Of course, it is straightforward to choose the overall normalization and phase of the threshold basis $\mathbf{E}_\pm$ such that the standing modes are still $\mathbf{E}_+ \pm \mathbf{E}_-$ and $\mathbf{E}_+ \pm i\mathbf{E}_-$, just as in the $C_{4\ell\mathrm{v}}$ case.

Appendix C: Stability calculations

In this appendix, we provide details for the derivation of the stability eigenvalues given in Sec. III B. Comparing Eq. (23) and Eq. (24), we see that the matrices are

$$\mathsf{A} = \begin{pmatrix} \Delta & -\varepsilon_\mathrm{I}\omega^2 & \omega^2 & 0 & 0 \\ \varepsilon_\mathrm{I}\omega^2 & \Delta & 0 & \omega^2 & 0 \\ \gamma_\perp D & 0 & \omega_a - \omega & \gamma_\perp & \gamma_\perp \mathbf{E}_\mathrm{R} \\ 0 & \gamma_\perp D & -\gamma_\perp & \omega_a - \omega & \gamma_\perp \mathbf{E}_\mathrm{I} \\ -\mathbf{P}_\mathrm{I} & \mathbf{P}_\mathrm{R} & \mathbf{E}_\mathrm{I} & -\mathbf{E}_\mathrm{R} & \gamma_\parallel \end{pmatrix}, \tag{C1}$$

where $\Delta = \varepsilon_\mathrm{R}\omega^2 - \nabla \times \nabla\times$, $\mathbf{E}_\mathrm{R} \equiv \mathrm{Re}(\mathbf{E})$, and $\mathbf{E}_\mathrm{I} \equiv \mathrm{Im}(\mathbf{E})$,

$$\mathsf{B} = \begin{pmatrix} -2\varepsilon_\mathrm{I}\omega & -2\varepsilon_\mathrm{R}\omega & 0 & -2\omega & 0 \\ 2\varepsilon_\mathrm{R}\omega & -2\varepsilon_\mathrm{I}\omega & 2\omega & 0 & 0 \\ 0 & 0 & 0 & 1 & 0 \\ 0 & 0 & -1 & 0 & 0 \\ 0 & 0 & 0 & 0 & 1 \end{pmatrix}, \tag{C2}$$

and

$$\mathsf{C} = \begin{pmatrix} -\varepsilon_\mathrm{R} & \varepsilon_\mathrm{I} & -1 & 0 & 0 \\ -\varepsilon_\mathrm{I} & -\varepsilon_\mathrm{R} & 0 & -1 & 0 \\ 0 & 0 & 0 & 0 & 0 \\ 0 & 0 & 0 & 0 & 0 \\ 0 & 0 & 0 & 0 & 0 \end{pmatrix}. \tag{C3}$$

We expand the matrices in powers of $\sqrt{d}$, as in Eq. (27), by noting that $\omega = \omega_\mathrm{t} + \omega_1 d + \mathcal{O}(d^2)$, $D_0 = D_\mathrm{t}(1+d)$, and $\mathbf{E}, \mathbf{P} = \mathcal{O}(\sqrt{d})$, according to Eq. (14). Now expand Eq. (25) and keep track of terms order-by-order using Eq. (28).

1. Zeroth and lowest ($d^{1/2}$) orders

At zeroth order, we have

$$\left(\mathsf{C}\sigma_0^2 + \mathsf{B}_0\sigma_0 + \mathsf{A}_0\right)\mathsf{x}_0 = 0, \tag{C4}$$

which turns out to be equivalent to the SALT equation at threshold, Eq. (13). The solution is easily seen to be any linear combination of the threshold modes (with the associated polarizations), given in Eq. (30). Because these modes already solve the SALT equation, they necessarily have $\sigma_0 = 0$ (there are other solutions to Eq. (C4), corresponding to the below-threshold modes. However, by definition, they are stable, so we are not concerned with them). Note that there are now four linearly-independent eigenvectors (from Eq. (30)), even though we only have a double degeneracy in the threshold modes. This is because we have separated the problem into real and imaginary parts, and this separation will become significant at higher orders in $\sqrt{d}$, when the non-analyticity appears in the equations.

Inserting these results into Eq. (25) at order $\sqrt{d}$, we have

$$\left(\mathsf{B}_0\sigma_{1/2} + \mathsf{A}_{1/2}\right)\sum b_k \mathsf{v}_k + \mathsf{A}_0 \mathsf{x}_{1/2} = 0. \tag{C5}$$

We now define the vectors

$$\mathsf{w}_j = \begin{pmatrix} \mathrm{Re}\mathbf{e}_j \\ -\mathrm{Im}\mathbf{e}_j \\ \omega_\mathrm{t}^2 \mathrm{Re}\left(\mathbf{e}_j \Gamma_\mathrm{t}\right)/\gamma_\perp \\ -\omega_\mathrm{t}^2 \mathrm{Im}\left(\mathbf{e}_j \Gamma_\mathrm{t}\right)/\gamma_\perp \\ 0 \end{pmatrix}. \tag{C6}$$

where $\mathbf{e}_k$ forms the four-component complex basis defined in Eq. (30). It is straightforward to show that $\mathsf{A}_0^T \mathsf{w}_j = 0$. Additionally, due to the nonzero pattern of $\mathsf{A}_{1/2}$, it is easy to see that $\mathsf{A}_{1/2}\mathsf{v}_k$ has all zero elements except the last, and hence $\mathsf{w}_j^T \mathsf{A}_{1/2}\mathsf{v}_k = 0$. Acting on Eq. (C5) with w_j^T, we then obtain $\sigma_{1/2} \sum \left(\mathsf{w}_j^T \mathsf{B}_0 \mathsf{v}_k\right) b_k = 0$. The matrix $\mathsf{w}_j^T \mathsf{B}_0 \mathsf{v}_k$ is nonsingular, which we will see later after we explicitly compute it in Eq. (C19). Hence, we conclude that $\sigma_{1/2} = 0$.

Next, we compute $\mathsf{A}_{1/2}\mathsf{v}_k$. Since the only nonzero element of $\mathsf{A}_{1/2}\mathsf{v}_k$ is the last, we define this element, after straightforward evaluation, as

$$g_k \equiv 2D_\mathrm{t} \left|\Gamma_\mathrm{t}\right| \sqrt{\gamma_\parallel} \mathrm{Re}\left[\mathbf{e}_k^\star \cdot \left(a_+ \mathbf{E}_+ + a_- \mathbf{E}_-\right)\right]. \tag{C7}$$

Inserting the result $\sigma_{1/2} = 0$ into Eq. (C5), we obtain

$$\mathsf{A}_0 \mathsf{x}_{1/2} = -\mathsf{A}_{1/2} \sum b_k \mathsf{v}_k = \begin{pmatrix} 0 \\ 0 \\ 0 \\ 0 \\ -\sum b_k g_k \end{pmatrix}. \tag{C8}$$

The vector $\mathsf{x}_{1/2}$ must also have this same nonzero pattern, because if it had any nonzero elements in the first four, they must be annihilated by A_0 and hence must be some linear combination of v_k (which is already accounted for in x_0 and would be redundant). Hence, we immediately conclude by inspection of A_0 that

$$\mathsf{x}_{1/2} = \begin{pmatrix} 0 \\ 0 \\ 0 \\ 0 \\ -\gamma_\parallel^{-1} \sum b_k g_k \end{pmatrix}. \tag{C9}$$

2. First order

At the next order, $\mathcal{O}(d)$, Eq. (25) is

$$\left(\mathsf{B}_0 \sigma_1 + \mathsf{A}_1\right) \sum b_k \mathsf{v}_k + \mathsf{A}_{1/2}\mathsf{x}_{1/2} + \mathsf{A}_0 \mathsf{x}_1 = 0. \tag{C10}$$

(Note that without the $\mathsf{A}_{1/2}\mathsf{x}_{1/2}$ term, Eq. (C10) would yield identical results to finding the two passive poles of the SALT equation that come from the threshold degenerate lasing modes.) Again, act on this equation with w_j^T. By direct evaluation, we have

$$\mathsf{w}_j^T \mathsf{A}_1 \mathsf{v}_k = \mathrm{Re}\left[\omega_1 \frac{\partial}{\partial \omega_\mathrm{t}} \omega_\mathrm{t}^2 \int d^3x\, \mathbf{e}_j \cdot \left(\varepsilon + \Gamma_\mathrm{t} D_\mathrm{t}\right) \mathbf{e}_k\right] + \mathrm{Re}\left[\omega_\mathrm{t}^2 \Gamma_\mathrm{t} \int d^3x\, D_\mathrm{t} \mathbf{e}_j \cdot \left(1 - \left|\mathbf{f}\right|^2\right) \mathbf{e}_k\right] \tag{C11}$$

and

$$\mathsf{w}_j^T \mathsf{B}_0 \mathsf{v}_k = -\mathrm{Im}\left[\frac{\partial}{\partial \omega_\mathrm{t}} \omega_\mathrm{t}^2 \int d^3x\, \mathbf{e}_j \cdot \left(\varepsilon + \Gamma_\mathrm{t} D_\mathrm{t}\right) \mathbf{e}_k\right]. \tag{C12}$$

By the same symmetry arguments used to evaluate the integrals in Appendix B, it is straightforward to show that

$$\frac{\partial}{\partial \omega_\mathrm{t}} \omega_\mathrm{t}^2 \int d^3x\, \mathbf{e}_j \cdot \left(\varepsilon + \Gamma_\mathrm{t} D_\mathrm{t}\right) \mathbf{e}_k = \omega_\mathrm{t}^2 \Gamma_\mathrm{t} H \begin{pmatrix} \mathsf{X} & i\mathsf{X} \\ i\mathsf{X} & -\mathsf{X} \end{pmatrix}_{jk}, \tag{C13}$$

where H is given in Eq. (B5) and

$$\mathsf{X} \equiv \begin{pmatrix} 0 & 1 \\ 1 & 0 \end{pmatrix}. \tag{C14}$$

Next, we have

$$\int d^3x\, D_\mathrm{t} \mathbf{e}_j \cdot \left|\mathbf{f}\right|^2 \mathbf{e}_k = \begin{pmatrix} \mathsf{M} & i\mathsf{M} \\ i\mathsf{M} & -\mathsf{M} \end{pmatrix}_{jk} + \left(\left|a_+\right|^2 I_+ + \left|a_-\right|^2 I_-\right) \begin{pmatrix} \mathsf{X} & i\mathsf{X} \\ i\mathsf{X} & -\mathsf{X} \end{pmatrix}_{jk} \tag{C15}$$

where

$$\mathsf{M} \equiv \begin{pmatrix} a_+^\star a_- J_+ + a_+ a_-^\star K_+ & 0 \\ 0 & a_+^\star a_- K_- + a_+ a_-^\star J_- \end{pmatrix}. \tag{C16}$$

Putting these results together, we have

$$\mathsf{w}_j^T \mathsf{A}_1 \mathsf{v}_k = \omega_\mathrm{t}^2 \mathrm{Re}\left[\Gamma_\mathrm{t} W \begin{pmatrix} \mathsf{X} & i\mathsf{X} \\ i\mathsf{X} & -\mathsf{X} \end{pmatrix}_{jk} - \Gamma_\mathrm{t} \begin{pmatrix} \mathsf{M} & i\mathsf{M} \\ i\mathsf{M} & -\mathsf{M} \end{pmatrix}_{jk}\right] \tag{C17}$$

where

$$W \equiv \omega_1 H + G_D - \left|a_+\right|^2 I_+ - \left|a_-\right|^2 I_-, \tag{C18}$$

and

$$\mathsf{w}_j^T \mathsf{B}_0 \mathsf{v}_k = -\omega_\mathrm{t}^2 \mathrm{Im}\left[\Gamma_\mathrm{t} H \begin{pmatrix} \mathsf{X} & i\mathsf{X} \\ i\mathsf{X} & -\mathsf{X} \end{pmatrix}_{jk}\right]. \tag{C19}$$

Next, by straightforward computation, we obtain

$$\mathsf{w}_j^T \mathsf{A}_{1/2}\mathsf{x}_{1/2} = -\sum_k b_k \int d^3x\, \omega_\mathrm{t}^2 D_\mathrm{t} \mathrm{Re}\left[\Gamma_\mathrm{t} \left(\mathbf{f} \cdot \mathbf{e}_j\right) \left(\mathbf{f} \cdot \mathbf{e}_k^\star + \mathbf{f}^\star \cdot \mathbf{e}_k\right)\right]. \tag{C20}$$

Again, by straightforward computation, we see that

$$\int d^3x\, D_\mathrm{t} \left(\mathbf{f} \cdot \mathbf{e}_j\right) \left(\mathbf{f} \cdot \mathbf{e}_k^\star\right) = \begin{pmatrix} \mathsf{Q} & -i\mathsf{Q} \\ i\mathsf{Q} & \mathsf{Q} \end{pmatrix}_{jk}$$
$$\int d^3x\, D_\mathrm{t} \left(\mathbf{f} \cdot \mathbf{e}_j\right) \left(\mathbf{f}^\star \cdot \mathbf{e}_k\right) = \begin{pmatrix} \mathsf{P} & i\mathsf{P} \\ i\mathsf{P} & -\mathsf{P} \end{pmatrix}_{jk} \tag{C21}$$

where

$$\mathsf{Q} \equiv \begin{pmatrix} a_+a_-(I_+ + J_+) & a_-^2 I_- + a_+^2 K_+ \\ a_+^2 I_+ + a_-^2 K_- & a_+a_-(I_- + J_-) \end{pmatrix}$$
$$\mathsf{P} \equiv \begin{pmatrix} a_-a_+^\star I_+ + a_+a_-^\star K_+ & |a_-|^2 I_- + |a_+|^2 J_+ \\ |a_+|^2 I_+ + |a_-|^2 J_- & a_+a_-^\star I_- + a_-a_+^\star K_- \end{pmatrix}. \tag{C22}$$

Putting this together, Eq. (C20) then becomes

$$\mathsf{w}_j^T \mathsf{A}_{1/2}\mathsf{x}_{1/2} = -\sum_k b_k\omega_{\rm t}^2 \mathrm{Re}\left[\Gamma_{\rm t}\begin{pmatrix} \mathsf{Q}+\mathsf{P} & i(\mathsf{P}-\mathsf{Q}) \\ i(\mathsf{P}+\mathsf{Q}) & \mathsf{Q}-\mathsf{P}\end{pmatrix}_{jk}\right]. \tag{C23}$$

Combining this with Eq. (C17) and Eq. (C19), defining $\tilde{\mathsf{P}} \equiv \mathsf{P}+\mathsf{M}-W\mathsf{X}$, and evaluating the real and imaginary components, Eq. (C10) becomes

$$\begin{pmatrix} \mathrm{Re}\left[\Gamma_{\rm t}(\mathsf{Q}+\tilde{\mathsf{P}})\right] & \mathrm{Im}\left[\Gamma_{\rm t}(\mathsf{Q}-\tilde{\mathsf{P}})\right] \\ -\mathrm{Im}\left[\Gamma_{\rm t}(\mathsf{Q}+\tilde{\mathsf{P}})\right] & \mathrm{Re}\left[\Gamma_{\rm t}(\mathsf{Q}-\tilde{\mathsf{P}})\right]\end{pmatrix}\mathsf{b} = -\sigma_1\begin{pmatrix} \mathrm{Im}(\Gamma_{\rm t}H)\mathsf{X} & \mathrm{Re}(\Gamma_{\rm t}H)\mathsf{X} \\ \mathrm{Re}(\Gamma_{\rm t}H)\mathsf{X} & -\mathrm{Im}(\Gamma_{\rm t}H)\mathsf{X}\end{pmatrix}\mathsf{b}. \tag{C24}$$

Using the fact that X is its own inverse, we multiply this equation by the matrix on the right-hand side, and obtain

$$\begin{pmatrix} \mathrm{Im}\left[\mathsf{X}(\mathsf{Q}+\tilde{\mathsf{P}})/H\right] & -\mathrm{Re}\left[\mathsf{X}(\mathsf{Q}-\tilde{\mathsf{P}})/H\right] \\ -\mathrm{Re}\left[\mathsf{X}(\mathsf{Q}+\tilde{\mathsf{P}})/H\right] & -\mathrm{Im}\left[\mathsf{X}(\mathsf{Q}-\tilde{\mathsf{P}})/H\right]\end{pmatrix}\mathsf{b} = \sigma_1\mathsf{b}, \tag{C25}$$

which is a 4×4 linear eigenvalue problem for σ_1.

3. Closed-form stability eigenvalues

We now diagonalize Eq. (C25) for each of the lasing mode solutions in Sec. III.

Circulating lasing mode

For the circulating solution in Eq. (18), we have $a_- = 0$, leading to $W = 0$ and $\tilde{\mathsf{P}} = \mathsf{P}$. The matrix in Eq. (C25) then becomes

$$\begin{pmatrix} 2\mathrm{Im}\left(\frac{I_+}{H}\right) & 0 & 0 & 0 \\ 0 & \mathrm{Im}\left(\frac{K_++J_+}{H}\right) & 0 & -\mathrm{Re}\left(\frac{K_+-J_+}{H}\right) \\ -2\mathrm{Re}\left(\frac{I_+}{H}\right) & 0 & 0 & 0 \\ 0 & -\mathrm{Re}\left(\frac{K_++J_+}{H}\right) & 0 & -\mathrm{Im}\left(\frac{K_+-J_+}{H}\right)\end{pmatrix}|a_+|^2, \tag{C26}$$

where $|a_+|^2 \equiv \frac{\omega_1 H + G_D}{I_+}$. By inspection, there is an eigenpair with

$$\sigma_1 = 0,\ \mathsf{b} = \begin{pmatrix} 0\\0\\1\\0\end{pmatrix}. \tag{C27}$$

Since the third component of the basis is $\mathbf{e}_3 = i\mathbf{E}_+$, this eigenvector corresponds to a global phase rotation $\mathbf{E}_+ \to (1+i\delta)\mathbf{E}_+$, which is a continuous symmetry of the original Maxwell–Bloch equations. A second eigenpair is

$$\sigma_1 = 2|a_+|^2\,\mathrm{Im}\left(\frac{I_+}{H}\right),\ \mathsf{b} = \begin{pmatrix} \mathrm{Im}\left(\frac{I_+}{H}\right)\\0\\-\mathrm{Re}\left(\frac{I_+}{H}\right)\\0\end{pmatrix}. \tag{C28}$$

The remaining two eigenvalues are

$$\sigma_1 = \left[\mathrm{Im}\left(\frac{J_+}{H}\right) \pm \sqrt{\left|\frac{K_+}{H}\right|^2 - \mathrm{Re}\left(\frac{J_+}{H}\right)^2}\right]|a_+|^2, \tag{C29}$$

with

$$\mathbf{b} = \begin{pmatrix} 0 \\ \mathrm{Re}\left(\frac{K_+-J_+}{H}\right) \\ 0 \\ \mathrm{Im}\left(\frac{K_+}{H}\right) \mp \sqrt{\left|\frac{K_+}{H}\right|^2 - \mathrm{Re}\left(\frac{J_+}{H}\right)^2}\end{pmatrix}. \tag{C30}$$

Standing-wave modes, $n \neq 4\ell$

We now diagonalize Eq. (C25) for the standing-wave modes. First, for $n \neq 4\ell$, standing-wave modes only occur in C_{nv}, as discussed in Appendix B. In this case, all $K_\pm = 0$, and $I_+, J_+ = I_-, J_-$. The matrix in Eq. (C25) then becomes $2|a|^2\times$

$$\begin{pmatrix} \mathrm{Im}\left(\frac{I}{H}\right) & \mathrm{Re}(z)\mathrm{Im}\left(\frac{I+J}{H}\right) & 0 & \mathrm{Im}(z)\mathrm{Im}\left(\frac{I+J}{H}\right) \\ \mathrm{Im}\left[z\left(\frac{I+J}{H}\right)\right] & \mathrm{Re}(z)\mathrm{Im}\left(\frac{I_z}{H}\right) & 0 & \mathrm{Im}(z)\mathrm{Im}\left(\frac{I_z}{H}\right) \\ -\mathrm{Re}\left(\frac{I}{H}\right) & -\mathrm{Re}(z)\mathrm{Re}\left(\frac{I+J}{H}\right) & 0 & -\mathrm{Im}(z)\mathrm{Re}\left(\frac{I+J}{H}\right) \\ -\mathrm{Re}\left[z\left(\frac{I+J}{H}\right)\right] & -\mathrm{Re}(z)\mathrm{Re}\left(\frac{I_z}{H}\right) & 0 & -\mathrm{Im}(z)\mathrm{Re}\left(\frac{I_z}{H}\right)\end{pmatrix}, \tag{C31}$$

where $|a|^2 = \frac{\omega_1 H + G_D}{2I+J}$. This matrix has *two* zero eigenvectors that have $\sigma_1 = 0$:

$$\mathsf{b} = \begin{pmatrix}0\\0\\1\\0\end{pmatrix},\ \mathsf{b} = \begin{pmatrix}0\\\mathrm{Im}(z)\\0\\\mathrm{Re}(z)\end{pmatrix}, \tag{C32}$$

which comes from the two continuous degrees of freedom in the solution: the overall global phase freedom, as well as the relative phase z in Eq. (19). It is straightforward to find the other two eigenpairs, which are

$$\sigma_1 = 2\mathrm{Im}\left(\frac{2I+J}{H}\right)|a|^2,\ \mathsf{b} = \begin{pmatrix}1\\\mathrm{Re}(z)\\0\\\mathrm{Im}(z)\end{pmatrix}, \tag{C33}$$

and

$$\sigma_1 = -2\mathrm{Im}\left(\frac{J}{H}\right)|a|^2,\ \mathsf{b} = \begin{pmatrix}-1\\\mathrm{Re}(z)\\0\\\mathrm{Im}(z)\end{pmatrix}. \tag{C34}$$

Standing-wave modes, $n = 4\ell$

Next, we examine the case $C_{n\mathrm{v}}$ for $n = 4\ell$ (standing-wave modes also exist here in the C_n case, but Eq. (C25) must be diagonalized numerically). For the case of a $\mathbf{E}_+ \pm \mathbf{E}_-$ lasing mode (Eq. (20)), the matrix in Eq. (C25) is $2|a|^2\times$

$$\begin{pmatrix} \mathrm{Im}\left(\frac{I}{H}\right) & \pm\mathrm{Im}\left(\frac{I+J+K}{H}\right) & -\mathrm{Re}\left(\frac{K}{H}\right) & \pm\mathrm{Re}\left(\frac{K}{H}\right) \\ \pm\mathrm{Im}\left(\frac{I+J+K}{H}\right) & \mathrm{Im}\left(\frac{I}{H}\right) & \pm\mathrm{Re}\left(\frac{K}{H}\right) & -\mathrm{Re}\left(\frac{K}{H}\right) \\ -\mathrm{Re}\left(\frac{I}{H}\right) & \mp\mathrm{Re}\left(\frac{I+J+K}{H}\right) & -\mathrm{Im}\left(\frac{K}{H}\right) & \pm\mathrm{Im}\left(\frac{K}{H}\right) \\ \mp\mathrm{Re}\left(\frac{I+J+K}{H}\right) & -\mathrm{Re}\left(\frac{I}{H}\right) & \pm\mathrm{Im}\left(\frac{K}{H}\right) & -\mathrm{Im}\left(\frac{K}{H}\right) \end{pmatrix}, \tag{C35}$$

where $|a|^2 = \frac{\omega_1 H + G_D}{2I+J+K}$, and the $\pm$ symbols correspond to $z = \pm 1$. There is a single zero eigenvalue:

$$\sigma_1 = 0,\ \mathsf{b} = \begin{pmatrix} 0 \\ 0 \\ 1 \\ \pm 1 \end{pmatrix}. \tag{C36}$$

A second eigenpair is

$$\sigma_1 = 2|a|^2\mathrm{Im}\left(\frac{2I+J+K}{H}\right),\ \mathsf{b} = \begin{pmatrix} 1 \\ \pm 1 \\ 0 \\ 0 \end{pmatrix}. \tag{C37}$$

Empirically, we have found that this eigenvalue is always stable. The final two eigenvalues are

$$\sigma_1 = -|a|^2\mathrm{Im}\left(\frac{J+3K}{H}\right) \pm |a|^2\sqrt{\mathrm{Im}\left(\frac{J-K}{H}\right)^2 - 8\mathrm{Re}\left(\frac{K}{H}\right)\mathrm{Re}\left(\frac{J+K}{H}\right)} \tag{C38}$$

(the eigenvectors can be written down in closed form, but are tedious and not illuminating). Empirically, we have found that at least one of these two eigenvalues are unstable (except for an isolated case, that we explain below). Next, for the case of a $\mathbf{E}_+ \pm i\mathbf{E}_-$ lasing mode (Eq. (21), the matrix in Eq. (C25) is $2|a|^2\times$

$$\begin{pmatrix} \mathrm{Im}\left(\frac{I}{H}\right) & \pm\mathrm{Re}\left(\frac{K}{H}\right) & \mathrm{Re}\left(\frac{K}{H}\right) & \pm\mathrm{Im}\left(\frac{I+J-K}{H}\right) \\ \pm\mathrm{Re}\left(\frac{I+J-K}{H}\right) & \mathrm{Im}\left(\frac{K}{H}\right) & \pm\mathrm{Im}\left(\frac{K}{H}\right) & \mathrm{Re}\left(\frac{I}{H}\right) \\ -\mathrm{Re}\left(\frac{I}{H}\right) & \pm\mathrm{Im}\left(\frac{K}{H}\right) & \mathrm{Im}\left(\frac{K}{H}\right) & \mp\mathrm{Re}\left(\frac{I+J-K}{H}\right) \\ \pm\mathrm{Im}\left(\frac{I+J-K}{H}\right) & -\mathrm{Re}\left(\frac{K}{H}\right) & \mp\mathrm{Re}\left(\frac{K}{H}\right) & \mathrm{Im}\left(\frac{I}{H}\right) \end{pmatrix}, \tag{C39}$$

where $|a|^2 = \frac{\omega_1 H + G_D}{2I+J-K}$, and the $\pm$ signs correspond to $z = \pm i$. There is an eigenpair with zero eigenvalue:

$$\sigma_1 = 0,\ \mathsf{b} = \begin{pmatrix} 0 \\ 1 \\ \mp 1 \\ 0 \end{pmatrix} \tag{C40}$$

and another eigenpair

$$\sigma_1 = 2|a|^2\mathrm{Im}\left(\frac{2I+J-K}{H}\right),\ \mathsf{b} = \begin{pmatrix} \pm 1 \\ 0 \\ 0 \\ 1 \end{pmatrix}. \tag{C41}$$

Empirically, we have found that this eigenvalue is always stable. Finally, the remaining two eigenvalues are

$$\sigma_1 = |a|^2\mathrm{Im}\left(\frac{3K-J}{H}\right) \pm |a|^2\sqrt{\mathrm{Im}\left(\frac{J+K}{H}\right)^2 + 8\mathrm{Re}\left(\frac{K}{H}\right)\mathrm{Re}\left(\frac{J-K}{H}\right)} \tag{C42}$$

(the eigenvectors can be written down in closed form, but are tedious and not illuminating). Empirically, we have found that at least one of these two eigenvalues are unstable, except for an isolated case that we will now explain.

We note that for the previous two cases, where $n = 4\ell$, it is possible to choose the shape of the gain profile $D_{\mathrm{t}}(\mathbf{x})$ such that $J = \pm K$, in which case the *one* of the two pairs $\mathbf{E}_+ \pm \mathbf{E}_-$ and $\mathbf{E}_+ \pm i\mathbf{E}_-$ actually becomes *stable*. To see this, we consider a $C_{n\mathrm{v}}$ geometry with $n = 4\ell$. Equation. (16) then becomes

$$\mathbf{E}_\pm = \sum_{b=1}^{n} (\pm i)^b R_{b/n}\mathbf{E}_{\mathrm{even}}. \tag{C43}$$

The specific choice of geometry requires that we place radially-symmetric lines of gain on the faces or diagonals of the $C_{n\mathrm{v}}$ geometry, which preserves the $C_{n\mathrm{v}}$ symmetry. We can write this as

$$D_{\mathrm{t}}(\mathbf{x}) = \sum_{a=1}^{n} G(r)\delta\left(\theta - \theta_a\right), \tag{C44}$$

where $\theta_a = \frac{2\pi a}{n}$ for the faces, and $\theta_a = (2a+1)\frac{\pi}{n}$ for the diagonals. For a TM geometry, we then have the overlap integrals (Eq. (B6))

$$J = \sum_{a=1}^{n}\int r dr\, G(r)\left|E_+\left(r,\theta_a\right)\right|^2 E_-(r,\theta_a)E_+(r,\theta_a)$$
$$K = \sum_{a=1}^{n}\int r dr\, G(r)E_+(r,\theta_a)^\star E_-(r,\theta_a)^3. \tag{C45}$$

It can be shown that depending on the choice of θ_a being the faces or diagonals, we will have either $K = J$ or $K = -J$. For $K = J$, the eigenvalues in Eq. (C42); of the $\mathbf{E}_+ \pm i\mathbf{E}_-$ standing-wave modes, become 0 and a stable eigenvalue. For $K = -J$, the same happens for those in Eq. (C38); of the $\mathbf{E}_+ \pm \mathbf{E}_-$ standing-wave modes.

4. Region of validity in small-$\gamma_\parallel$ limit

In this section, we work out the $\gamma_\parallel$ dependence of higher-order terms in the perturbation theory, and demonstrate that the regime of validity of the perturbation theory depends on d being small compared to a constant multiple of $\gamma_\parallel$. We show that the exact expansion of σ/d to all orders in d only contains terms of

the form $d^\ell/\gamma_\parallel^j$ with $\ell \geq j$, and that in the limit where $\gamma_\parallel, d \to 0$, with d vanishing at least as rapidly as $\gamma_\parallel$, the terms with $\ell > j$ vanish and the stability eigenvalue takes the asymptotic functional form $\sigma/d = f(d/\gamma_\parallel)$. Here, $f(0)$ is exactly the first-order stability eigenvalue σ_1. For circulating modes that have $\mathrm{Re}(\sigma_1) < 0$, the the smallest positive solution z_0 of the equation $\mathrm{Re}[f(z)] = 0$ gives a boundary of stability, for which a circulating lasing mode becomes *unstable* for $d > \gamma_\parallel z_0$, as seen in the ring-laser example in Ref. [7].

First, since we have already obtained closed-form expressions for σ_1 and the coefficients b_k of x_0, Eq. (C10) can be solved for x_1: $\mathsf{x}_1 = \mathsf{A}_0^{-1}\left[(\mathsf{B}_0\sigma_1 + \mathsf{A}_1)\,\mathsf{x}_0 + \mathsf{A}_{1/2}\mathsf{x}_{1/2}\right]$. Next, at order $d^{3/2}$, we have

$$\mathsf{A}_{3/2}\mathsf{x}_0 + \mathsf{A}_1\mathsf{x}_{1/2} + \mathsf{A}_{1/2}\mathsf{x}_1 + \mathsf{A}_0\mathsf{x}_{3/2} = -\mathsf{B}_0\sigma_{3/2}\mathsf{x}_0 - \mathsf{B}_0\sigma_1\mathsf{x}_{1/2}. \quad \text{(C46)}$$

The first three terms on the left-hand side as well as the very last term on the right all have the same nonzero pattern as $\mathsf{x}_{1/2}$. Hence, multiplying both sides by x_0^T (which is now known after having solved the degenerate problem at order d), we obtain $0 = \sigma_{3/2}\mathsf{x}_0^T\mathsf{B}_0\mathsf{x}_0$, which leads to $\sigma_{3/2} = 0$. The only remaining unknown is then $\mathsf{x}_{3/2}$. By the same arguments leading to Eq. (C9), we have $\mathsf{A}_0\mathsf{x}_{3/2} = \gamma_\parallel\mathsf{x}_{3/2}$, which yields $\mathsf{x}_{3/2} = -\gamma_\parallel^{-1}\mathsf{f}_{3/2}$, where

$$\mathsf{f}_{3/2} \equiv \mathsf{A}_{3/2}\mathsf{x}_0 + \mathsf{A}_1\mathsf{x}_{1/2} + \mathsf{A}_{1/2}\mathsf{x}_1 + \mathsf{B}_0\sigma_1\mathsf{x}_{1/2}, \quad \text{(C47)}$$

and $\mathsf{f}_{3/2}$ is $\mathcal{O}(1)$ with respect to $\gamma_\parallel$, i.e. it goes to a constant as $\gamma_\parallel \to 0$. Moving onto order d^2, we have

$$\mathsf{C}\sigma_1^2\mathsf{x}_0 + \mathsf{B}_0\left(\sigma_2\mathsf{x}_0 + \sigma_1\mathsf{x}_1\right) + \mathsf{B}_1\sigma_1\mathsf{x}_0 = -\sum_{k=0}^{4}\mathsf{A}_{k/2}\mathsf{x}_{2-\frac{k}{2}}. \quad \text{(C48)}$$

Multiplying both sides by x_0^T annihilates the $k = 0$ term, leaving only a single unknown σ_2 and a single term of $\mathcal{O}(\gamma_\parallel^{-1})$: $-\mathsf{A}_{1/2}\mathsf{x}_{3/2} = \gamma_\parallel^{-1}\mathsf{A}_{1/2}\mathsf{f}_{3/2}$. We then have

$$\gamma_\parallel\sigma_2 = \frac{\mathsf{x}_0^T\mathsf{A}_{1/2}\mathsf{f}_{3/2}}{\mathsf{x}_0^T\mathsf{B}_0\mathsf{x}_0} + \mathcal{O}(\gamma_\parallel). \quad \text{(C49)}$$

Carrying on to the next order results in $\sigma_{5/2} = 0$ and $\mathsf{x}_{5/2} = -\gamma_\parallel^{-1}\mathsf{f}_{5/2}$, where now $\mathsf{f}_{5/2} = \mathcal{O}(\gamma_\parallel^{-1})$ due to it including terms with σ_2 and x_2. By continuing this process, we find that $\sigma_{m+\frac{1}{2}} = 0$, and $\mathsf{x}_{m+\frac{1}{2}}$, σ_{m+1}, and x_{m+1} are all $\mathcal{O}(\gamma_\parallel^{-m})$. This is made possible by the fact that the only place $\gamma_\parallel$ occurs in the entire problem is the very last matrix element of A_0 in Eq. (C1), as well as the fact that the $\mathsf{x}_{m+\frac{1}{2}}$ and x_m have predictable nonzero patterns, due to the nonzero patterns of $\mathsf{A}_{m+\frac{1}{2}}$ being different from those of all the other matrices. Defining $s_{m+1} \equiv \gamma_\parallel^m\sigma_{m+1} = \mathcal{O}(1)$, we obtain a full expansion for the exact Maxwell–Bloch eigenvalue (Eq. (28)):

$$\sigma \approx d\sum_{k=1}^{\infty}\left(\frac{d}{\gamma_\parallel}\right)^{k-1}s_k, \quad \text{(C50)}$$

where the $\approx$ comes from the fact that we have thrown away terms of the form $d^\ell/\gamma_\parallel^j$ with $\ell > j$, which are negligible compared to $(d/\gamma_\parallel)^k$ and vanish in the limit $d, \gamma_\parallel \to 0$ (provided that $\gamma_\parallel$ does not go zero more rapidly than d). In this limit, we can then infer a generic functional form of σ:

$$\lim_{\gamma_\parallel, d\to 0}\frac{\sigma}{d} = f\left(\frac{d}{\gamma_\parallel}\right), \quad \text{(C51)}$$

where f is a complex-valued function (with a real argument) whose Taylor expansion is the sum in Eq. (C50). For an eigenvalue σ of the Maxwell–Bloch equation linearized about a circulating mode, we have $f(0) = \sigma_1$ having a negative real part. The smallest positive zero z_0 of $\mathrm{Re}f$ then gives the equation for a boundary of stability $d = \gamma_\parallel z_0$. Hence, in the limit that both $\gamma_\parallel$ and d go to zero, the region of stability for a circulating mode is given by $d < \gamma_\parallel z_0$, where z_0 is a constant independent of $\gamma_\parallel$ and d.

Appendix D: Determining the dielectric perturbation $\delta\varepsilon$

In this Appendix, we describe the processe used to force a degeneracy in a geometry whose symmetry has been broken by the discretization scheme (e.g., a C_{6v} geometry discretized into a rectangular grid). We first analyze the effect of a small $\delta\varepsilon$ on the eigenfrequencies (of the lasing mode and the passive pole) by well-known first-order perturbation theory for Maxwell's equations [33] (some modification is required to handle the nonlinearity of the hole-burning term above threshold). However, we first force the degeneracy below threshold (repeating as needed as the pump strength is increased), so that both passive poles reach threshold simultaneously. (In practice, we achieved the fastest convergence by allowing passive poles to have positive imaginary parts, and then setting the pump strength so that the two poles "straddle" the real axis; this way, when they meet in the middle they are both exactly at threshold.) Below threshold, the eigenproblem is linear in the eigenvector $\mathbf{E}$ (the nonlinearity in ω is still present but easy to deal with using standard methods), and we can apply standard perturbation theory (albeit for a complex-symmetric operator, not a Hermitian operator) as follows:

Consider two nonlasing modes that satisfy

$$0 = -\nabla\times\nabla\times\mathbf{E}_\mu + \omega_\mu^2\varepsilon_\mu\mathbf{E}_\mu$$
$$\varepsilon_\mu \equiv \varepsilon_c + D_\mathrm{t}\Gamma(\omega_\mu) \quad \text{(D1)}$$

Adding a perturbation to the dielectric $\delta\varepsilon$ will result in corresponding responses $\delta\mathbf{E}_\mu$ and $\delta\omega_\mu$. As in the threshold perturbation theory, we multiply both sides by $\mathbf{E}_\mu$

and keep only first-order terms. Terms involving $\delta\mathbf{E}_\mu$ again vanish because the operators act to the left, and we are left with [49, 53, 54]

$$\delta\omega_\mu = -\frac{\int d^3x\, \mathbf{E}_\mu \cdot \delta\varepsilon \mathbf{E}_\mu}{\int d^3x\, \mathbf{E}_\mu \cdot \left(\frac{2\varepsilon_\mu}{\omega_\mu} + \frac{\partial\varepsilon_\mu}{\partial\omega_\mu}\right)\mathbf{E}_\mu}. \tag{D2}$$

We write this frequency shift as an inner product

$$\delta\omega_\mu = -p_\mu^T \delta\varepsilon. \tag{D3}$$

As an aside, while it is fine to use a scalar $\delta\varepsilon$ function for this procedure, in the case when the $\mathbf{E}_\mu$ are TE modes or fully-vectorial fields, then it is also possible to allow $\delta\varepsilon(\mathbf{x})$ to be a diagonally anisotropic tensor

$$\overleftrightarrow{\delta\varepsilon}(\mathbf{x}) = \begin{pmatrix} \delta\varepsilon_{xx}(\mathbf{x}) & 0 & 0 \\ 0 & \delta\varepsilon_{yy}(\mathbf{x}) & 0 \\ 0 & 0 & \delta\varepsilon_{zz}(\mathbf{x}) \end{pmatrix}. \tag{D4}$$

The column-vector form of $\delta\varepsilon$ in Eq. (D3) would then have as its elements all the real and imaginary components of $\overleftrightarrow{\delta\varepsilon}(\mathbf{x})$ at each Yee point [36] [$\delta\varepsilon_{xx}(\mathbf{x})$, $\delta\varepsilon_{yy}(\mathbf{x})$, and $\delta\varepsilon_{zz}(\mathbf{x})$ for all the grid points $\mathbf{x}$], while the row-vector p_μ^T would have as its elements the real and imaginary parts of $E_x(\mathbf{x})^2$, $E_y(\mathbf{x})^2$, and $E_z(\mathbf{x})^2$ at all the grid points. If we take this option, then the norm we minimize would be

$$\|\delta\varepsilon\|_2^2 = \int d^3x \left\|\overleftrightarrow{\delta\varepsilon}(\mathbf{x})\right\|_F^2, \tag{D5}$$

where the Frobenius norm [55] at each point $\mathbf{x}$ is defined as

$$\left\|\overleftrightarrow{\delta\varepsilon}(\mathbf{x})\right\|_F^2 \equiv |\delta\varepsilon_{xx}(\mathbf{x})|^2 + |\delta\varepsilon_{yy}(\mathbf{x})|^2 + |\delta\varepsilon_{zz}(\mathbf{x})|^2. \tag{D6}$$

Whether we take $\delta\varepsilon$ to be a scalar or a tensor, the degeneracy-forcing condition $\omega_1 + \delta\omega_1 = \omega_2 + \delta\omega_2$ then becomes

$$(p_2 - p_1)^T \delta\varepsilon = \omega_2 - \omega_1. \tag{D7}$$

It turns out that the solution of a quadratic program with equality constraints can be obtained directly by solving a linear *dual* problem [34], which in this case is

$$\begin{pmatrix} 1 & 0 & q^R & q^I \\ 0 & 1 & -q^I & q^R \\ \left(q^R\right)^T & -\left(q^I\right)^T & 0 & 0 \\ \left(q^I\right)^T & \left(q^R\right)^T & 0 & 0 \end{pmatrix} \begin{pmatrix} \delta\varepsilon^R \\ \delta\varepsilon^I \\ \lambda_1 \\ \lambda_2 \end{pmatrix} = \begin{pmatrix} 0 \\ 0 \\ \omega_2^R - \omega_1^R \\ \omega_2^I - \omega_1^I \end{pmatrix}. \tag{D8}$$

Here, the superscripts ^{R} and ^{I} denote real and imaginary parts, and we have defined $q \equiv p_2 - p_1$, and the $\lambda_{1,2}$ are Lagrange multipliers that are not needed. When ω_2 is very close to ω_1, we can improve the condition number of the matrix by freely multiplying the second-to-last row and column of the matrix by a constant factor, provided that the second-to-last element of the right-hand side is *divided* by the same factor. The same can be done for the last row and column, with the last element of the right-hand side.

Note that even after the thresholds and threshold frequencies have been made exactly degenerate using the QP procedure illustrated above, we are still in principle forcing the degeneracy. Above threshold, the delicate balance created by $\delta\varepsilon$ to force the frequencies together is slightly broken. This results in an *approximate* degeneracy that is maintained very far above threshold, as shown in Fig. (10), with only a 10^{-8} splitting for pump strengths up to 100 times threshold. In practice, these results are already accurate enough to give all the desired physical information about the degenerate pair. If we wanted to be absolutely correct and force the degeneracy to machine precision (as it was in the exactly symmetric case for odd-ℓ modes), we could simply perform QP again at some given $d > 0$ to force $\delta\omega$ and $\delta\omega'$ back together. One extra caveat in this case is that $\delta\omega$ is now a lasing pole, so the spatial hole-burning term needs to be accounted for in the perturbation theory ($\delta\omega'$ is still a passive pole, so the previous perturbation theory still applies), and instead of Eq. (D2) we now have

$$\begin{aligned} \delta\omega &= -\frac{\int d^3x\, \mathbf{E}\cdot(\delta\varepsilon + D_\mathrm{t}\Gamma(\omega_\mu)\delta H)\,\mathbf{E}}{\int d^3x\, \mathbf{E}\cdot\left(\frac{2\varepsilon}{\omega} + \frac{\partial\varepsilon}{\partial\omega}\right)\mathbf{E}} \\ \varepsilon &\equiv \varepsilon_c + D_\mathrm{t}\Gamma(\omega)H \\ \delta H &\equiv \frac{1}{1+|\mathbf{E}+\delta\mathbf{E}|^2} - \frac{1}{1+|\mathbf{E}|^2}. \end{aligned} \tag{D9}$$

Here, δH is the change in the spatial-hole burning term arising from the dielectric perturbation $\delta\varepsilon$. However, since there is no easy way to determine $\delta\mathbf{E}$ without numerically solving the full problem, δH is hard to determine semi-analytically. A simple work-around is to set $\delta H = 0$ above, which makes this procedure no longer a true first-order perturbation theory. However, since the splitting is already so small as shown in Fig. (10), the $\delta\varepsilon$ needed is also extremely small, so δH is also negligible. Although $\delta\omega$ is not zero to first order, the $\delta H = 0$ approximation is enough to find a $\delta\varepsilon$ that greatly decreases $\delta\omega$. We find empirically that it usually takes one iteration of this above-threshold QP procedure to restore the degeneracy of the lasing pole ω and its passive mode ω' to machine precision, since $\delta\omega$ is already very small. Practically speaking, this entire extra step is rarely needed since the solutions obtained from $\delta\varepsilon$ for the linear problem below threshold are already close enough for most pump strengths of physical interest.

[1] H. Cao and J. Wiersig, Rev. Mod. Phys. **87** (2015).
[2] L. Ge, D. Liu, S. G. Johnson, S. Rotter, H. E. Türeci, H. Cao, A. Cerjan, and A. D. Stone, arXiv:1504.08018 (2015).
[3] V. S. Ilchenko and A. B. Matsko, IEEE J. Sel. Topics Quantum Electron. **12**, 3 (2006).
[4] Q. J. Wang, C. Yan, N. Yu, J. Unterhinninghofen, J. Wiersig, C. Pflugl, L. Diehl, T. Edamurac, M. Yamanishic, H. Kanc, and F. Capasso, Proc. Natl. Acad. Sci. USA **107**, 22407 (2005).
[5] T. Inui, Y. Tanabe, and Y. Onodera, *Group Theory and Its Applications in Physics* (Springer, 1996).
[6] H. Altug, D. Englund, and J. Vuckovic, Nat. Phys. **2**, 484 (2006).
[7] S. Burkhardt, M. Liertzer, D. O. Krimer, and S. Rotter, Phys. Rev. A **92** (2015).
[8] H. E. Türeci, A. D. Stone, and B. Collier, Phys. Rev. A **74**, 043822 (2006).
[9] H. E. Türeci, L. Ge, S. Rotter, and A. D. Stone, Science **320**, 643 (2008).
[10] H. Türeci, A. D. Stone, L. Ge, S. Rotter, and R. J. Tandy, Nonlinearity **22**, C1–C18 (2009).
[11] L. Ge, R. J. Tandy, A. D. Stone, and H. E. Türeci, Opt. Express **16**, 16895 (2008).
[12] L. Ge, Y. D. Chong, and A. D. Stone, Phys. Rev. A **82**, 063824 (2010).
[13] B. Hopkins, A. N. Poddubny, A. E. Miroshnichenko, T. J. Davis, and Y. S. Kivshar, Laser and Photonics Reviews **10**, 137 (2016).
[14] S. Esterhazy, D. Liu, M. Liertzer, A. Cerjan, K. G. Makris, A. D. Stone, J. M. Melenk, S. G. Johnson, and S. Rotter, Phys. Rev. A **90**, 023816 (2014).
[15] H. Risken and K. Nummedal, Phys. Lett. **26A** (1968).
[16] H. Zeghlache, P. Mandel, N. B. Abraham, L. M. Hoffer, G. L. Lippi, and T. Mello, Phys. Rev. A **37** (1987).
[17] L. A. Lugiato, L. M. Narducci, and M. F. Squicciarini, Phys. Rev. A **34** (1986).
[18] L. A. Lugiato, F. Prati, L. M. Narducci, and G. L. Oppo, Opt. Commun. **69** (1988).
[19] C. Tamm, Phys. Rev. A **38** (1988).
[20] L. A. Lugiato, C. Oldano, and L. M. Narducci, J. Opt. Soc. Am. B **5**, 879 (1988).
[21] M. Tinkham, *Group Theory and Quantum Mechanics*, 2nd ed. (Dover, 2003).
[22] H. Haken, *Laser Theory* (Springer, 1970).
[23] H. Haken and H. Sauermann, Z. Phys. **173** (1963).
[24] H. Haken, *Light: Laser light dynamics* (North-Holland Pub. Co., 1985).
[25] W. E. Lamb, Phys. Rev. **134** (1964).
[26] H. Fu and H. Haken, Phys. Rev. A **43**, 2446 (1991).
[27] I. Braun, G. Ihlein, F. Laeri, J. U. Nöckel, G. Schulz-Ekloff, F. Schüth, U. Vietze, Ö. Weiss, and D. Wöhrle, Appl. Phys. B **70**, 335 (2000).
[28] K. Sakoda, *Optical Properties of Photonic Crystals*, 2nd ed. (Springer, 2005).
[29] M. Sorel, G. Giuliani, A. Scire, R. Miglierina, S. Donati, and P. J. R. Laybourn, IEEE J. Quantum Electron. **39**, 1187 (2003).
[30] F. Tisseur and K. Meerbergen, SIAM Rev. **43**, 235 (2001).
[31] J. J. Sakurai, *Modern Quantum Mechanics* (Addison Wesley, 1993).
[32] G. Strang, *Introduction to Linear Algebra* (Wellesley Cambridge Press, 2009).
[33] J. D. Joannopoulos, S. G. Johnson, J. N. Winn, and R. D. Meade, *Photonic Crystals: Molding the Flow of Light*, 2nd ed. (Princeton, 2008).
[34] S. Boyd and L. Vandenberghe, *Convex Optimization* (Cambridge Univ. Press, 2004).
[35] N. J. Champagne, J. G. Berryman, and H. M. Buettner, J. Comp. Phys. **170**, 830 (2001).
[36] A. Taflove and S. C. Hagness, *Computational Electrodynamics: The Finite-Difference Time-Domain Method*, 3rd ed. (Artech House, 2005).
[37] A. Farjadpour, D. Roundy, A. Rodriguez, M. Ibanescu, P. Bermel, J. D. Joannopoulos, and S. G. Johnson, Opt. Lett. **31**, 2972 (2006).
[38] L. Ge, H. Cao, and A. D. Stone, "Condensation of thresholds in multimode lasers," (2016), arXiv:1607.08204.
[39] K. Iga, IEEE J. Sel. Topics Quantum Electron. **6**, 1201 (2000).
[40] W. Schrenk, N. Finger, S. Gianordoli, L. Hvozdara, G. Strasser, and E. Gornik, Appl. Phys. Lett. **77**, 2086 (2000).
[41] G. A. Turnbull, P. Andrew, M. J. Jory, W. L. Barnes, and I. D. W. Samuel, Phys. Rev. B **64** (2001).
[42] P.Andrew, G. A. Turnbull, I. D. W. Samuel, and W. L. Barnes, Appl. Phys. Lett. **81**, 954 (2002).
[43] M. Imada, A. Chutinan, S. Noda, and M. Mochizuki, Phys. Rev. B **65** (2002).
[44] G. Vecchi, F. Raineri, I. Sagnes, A. Yacomotti, P. Monnier, T. J. Karle, K.-H. Lee, R. Braive, L. L. Gratiet, S. Guilet, G. Beaudoin, A. Talneau, S. Bouchoule, A. Levenson, and R. Raj, Opt. Express **15**, 7551 (2003).
[45] H.-Y. Ryu, S.-H. Kwon, Y.-J. Lee, Y.-H. Lee, and J.-S. Kim, Appl. Phys. Lett. **80**, 3476 (2002).
[46] M. Imada, S. Noda, A. Chutinan, T. Tokudac, M. Murata, and G. Sasaki, Appl. Phys. Lett. **75**, 316 (1999).
[47] A. Yariv, *Quantum Electronics*, 3rd ed. (Wiley, 1989).
[48] N. W. Ashcroft and N. D. Mermin, *Solid State Physics* (Cengage Learning, 1978).
[49] A. Pick, A. Cerjan, D. Liu, A. W. Rodriguez, A. D. Stone, Y. D. Chong, and S. G. Johnson, Phys. Rev. A **91** (2015).
[50] N. Moiseyev, *Non-Hermitian Quantum Mechanics* (Cambridge, 2011).
[51] A. E. Siegman, in *Frontiers of Laser Physics and Quantum Optics*, edited by Z. Xu, S. Xie, S. Y. Zhu, and M. O. Scully (Springer–Verlag, 1994) pp. 31–37.
[52] J. R. Schulenberger and C. H. Wilcox, Arch. Ration. Mech. Anal **41** (1971).
[53] A. Raman and S. Fan, Phys. Rev. B **83** (2011).
[54] M. Soljačić, E. Lidorikis, L. V. Hau, and J. D. Joannopoulos, Phys. Rev. E **71** (2005).
[55] L. N. Trefethen and D. Bau, *Numerical Linear Algebra* (SIAM, 1997).